

Cosmic shielding studies at MicroBooNE

M. Bass, D. Caratelli, E. Church, B. Eberly, S. Gollapinni, R. Grosso,
A. Hackenburg, G. Horton-Smith, V. Paolone and T. Yang

January 5, 2016

Abstract

Recently, there has been a great concern over the size of cosmogenic backgrounds expected in liquid argon-based surface detectors. Since MicroBooNE is located only a few meters below the surface, a large flux of cosmic rays is expected to enter the detector volume. One of the most effective ways to reduce cosmic air shower background is to use a high-density shielding material a few meters above the detector to block the incoming cosmic particles. Through detailed Monte Carlo simulations, this technote addresses the question of whether MicroBooNE would require an overburden or not. The size of various cosmic backgrounds expected in the detector is estimated and the effect of a 3 m concrete overburden on these backgrounds is studied in detail. Special focus is given to estimating cosmogenic electromagnetic showers that can fake a ν_e -like event and pose a serious challenge to studies involving single e/γ searches. Based on the studies presented in this note, it is strongly recommended that MicroBooNE install a concrete overburden of at least 2 m thickness to reliably control cosmic non-muon induced backgrounds.

17 Contents

18	1 Introduction	3
19	2 MicroBooNE Geometry simulation	3
20	3 Cosmic RaY generator (CRY)	5
21	3.1 CRY in LArSoft	6
22	3.2 CRY Muon flux validation	7
23	3.3 Other issues in cosmic simulation	9
24	4 CORSIKA Cosmic ray simulations	11
25	4.1 Running & Interfacing with CORSIKA	12
26	4.2 Flux Comparisons between CORSIKA and CRY	14
27	4.3 The CMC Model	14
28	5 Analysis framework and data samples	15
29	6 Simulated particle rates	17
30	6.1 Cosmogenic ν_e -like backgrounds	19
31	7 The effect of an overburden	22
32	7.1 Effect of overburden on cosmogenic ν_e -like backgrounds	25
33	7.2 Secondary production in the overburden	25
34	7.3 Overburden size recommendation	26
35	8 Summary and conclusions	27
36	9 Acknowledgments	29
37	Appendix A Neutron and Proton scattering in Geant4	31
38	Appendix B Neutron “Killer” processes in LArG4	32

1 Introduction

In surface-based particle detectors, cosmic backgrounds are a great concern. Since MicroBooNE is situated just below the surface (only ~ 6 meters underground), it will be exposed to a large flux of cosmic rays. Estimating the portion of this cosmic flux that enters the detector and exploring ways to reduce it are crucial to successfully perform any beam-related analysis at MicroBooNE. Understanding these backgrounds would not only benefit MicroBooNE but the entire short-baseline neutrino (SBN) physics program at Fermilab.

One way to reduce primary cosmic background in surface detectors is to introduce an earth-equivalent (density-wise) overburden on the roof enclosure of the detector hall. The purpose of this technote is to determine whether MicroBooNE requires an overburden. Addressing this question requires understanding the size of various primary and secondary cosmic backgrounds that will enter the active volume of the detector. In particular, estimating the cosmic electromagnetic (EM) background is crucially important for single e/γ searches and to address the low energy excess observed by the MiniBooNE experiment.

All the studies shown in this technote are performed using detailed Monte Carlo (MC) simulations. Details about the geometry simulation of the detector enclosure, surrounding materials, and the overburden configuration that is used in these studies are given in Section 2. Two MC generators, CRY [1] and CORSIKA [2], are used to generate cosmic ray data samples. These are described in Sections 3 and 4. Limitations of the CRY generator software are also discussed. While doing these studies, we discovered some bugs in the CRY integration software that resulted in significantly lower muon and hadron flux estimates. Section 3 gives details about the integration software and problems associated with it. The analysis framework and cosmic data samples used in this study are explained in Section 5.

Estimates of primary and secondary particle rates expected in the detector active volume are presented in Section 6. Initial studies show that choosing a 3 m concrete overburden can drastically reduce some of the primary cosmic non-muon backgrounds. Muons, however, can easily penetrate through the shielding material and enter the detector volume. Not only these primary muons themselves are a background to many physics studies (like the muon-neutrino cross-section analysis), but they also induce energetic EM showers inside the detector. Detailed estimates of these cosmic-induced EM showers are shown in Section 6. The effect of using a 3 m concrete overburden on various backgrounds is discussed in Section 7. Section 8 gives a summary of the studies presented in the technote and reiterates important observations to determine whether MicroBooNE would benefit from an overburden.

2 MicroBooNE Geometry simulation

This section briefly describes the MicroBooNE geometry that is currently used in the simulation. The MicroBooNE geometry simulation is at a mature stage and includes detailed simulations of the detector, cryostat and surroundings. Elements that surround the detector and have non-negligible density are important for cosmic background studies since they can absorb some particles and generate additional backgrounds. For example, the electronics racks that are located just above the detector on the platform can block significant amounts of cosmic electromagnetic background, while the dense concrete experimental pit that surrounds the cryostat is capable of producing new backgrounds due to particle interactions in the concrete.

According to LArTF building engineers, the building is designed to hold up to 3 meters of concrete-equivalent overburden. Currently for the overburden simulation, we assume a uniform 3 m thick concrete

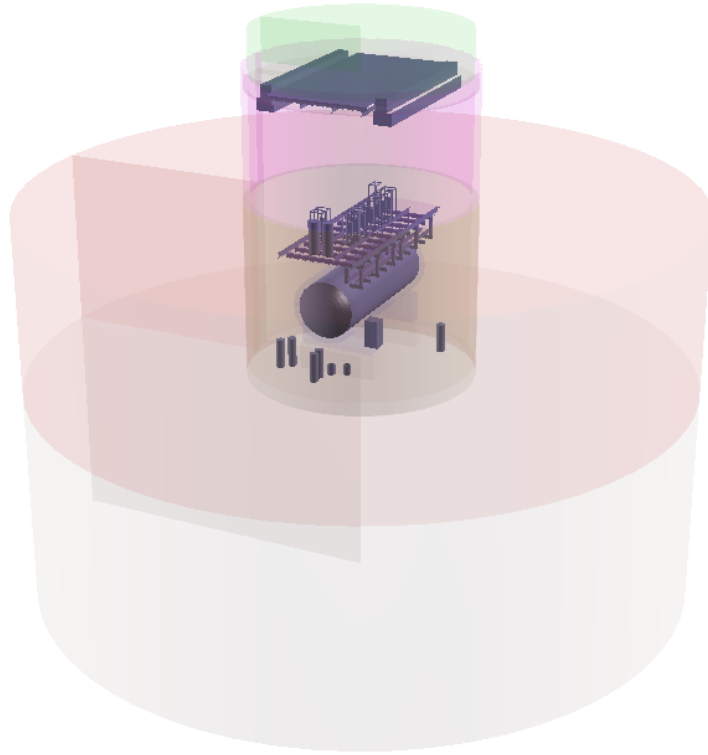


Figure 1: MicroBooNE geometry simulation of the detector and its surroundings. In order to clearly show the details of the simulation, a transparent view of the geometry is shown. The green disc located on the roof of the building shows the overburden.

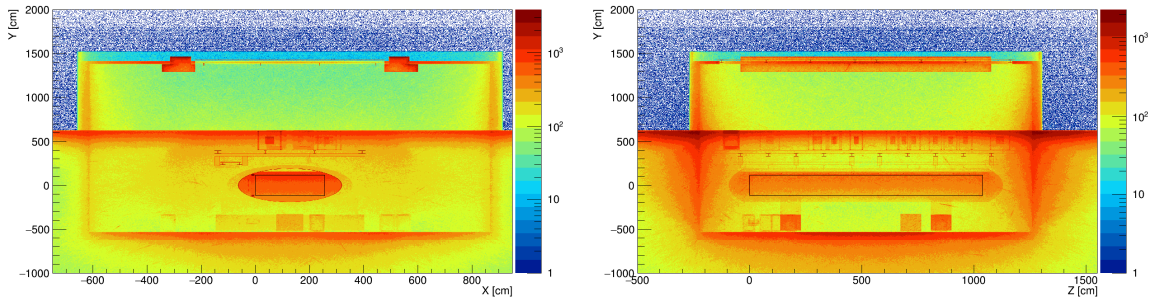


Figure 2: End point distribution of all cosmic particles using a data sample with no overburden simulation in YX projection (left) and YZ projection (right) of the MicroBooNE geometry.

84 disc placed above the roof of the LArTF building. Note that this assumption, although a good approx-
 85 imation, is not realistic since multiple concrete blocks will be used to cover the roof of the LArTF
 86 building, so, the coverage won't be as uniform as the concrete disc. Figure 1 shows a transparent view
 87 of the MicroBooNE geometry with overburden included.

88

89 One way to verify the simulated geometry is to plot the stopping point positions of all cosmic
 90 particles. Figure 2 shows the end-point distributions of all cosmic particles in YX (left) and YZ (right)
 91 projected planes of the MicroBooNE TPC without the overburden simulation. Figure 3 shows the same
 92 set of plots but with the 3 m overburden simulation. The figures clearly show most of the details of the
 93 simulated geometry.

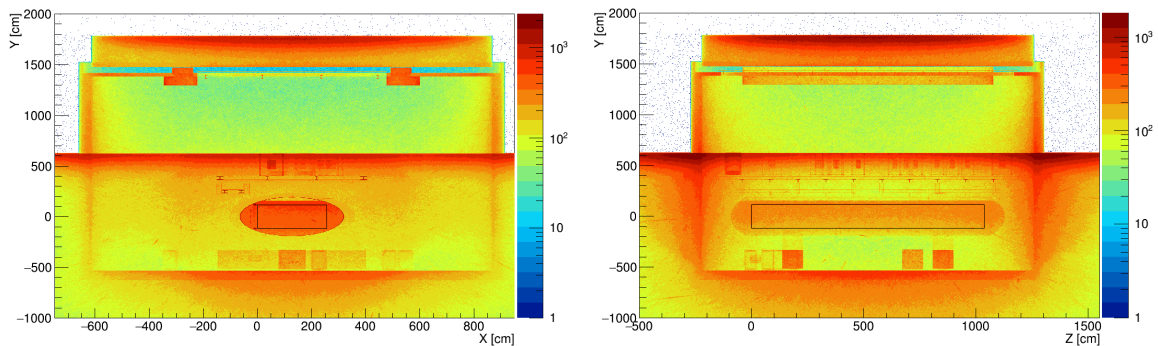


Figure 3: End point distribution of all cosmic particles using a data sample with 3 m concrete overburden simulation in YX projection (left) and YZ projection (right) of the MicroBooNE geometry. Note that the reason there are only few end points outside LArTF (compared to Fig. 2) is because the region above ground and outside LArTF is filled with vacuum in this sample. This is a minor inconsistency and won't affect the conclusions in any way since the particles are only projected from 18 m.

3 Cosmic RaY generator (CRY)

The CRY [1] MC generator is capable of generating all particle (and anti-particle) types at one of three altitudes: sea level, 2100 m and 11300 m. There is no provision in CRY yet to specify an intermediate value between the three standard elevation points. Because of this, even though Fermilab is at an elevation of 740.6 feet (~ 226 m) above mean sea level, all MC samples generated are at sea level. Following Equations (1) and (2) of Ref. 8, one can compute the relative increase in particle fluxes with respect to sea level to get an estimate of how flux varies with altitude. Table 1 shows the anticipated increase in flux at 226 m and 750 m¹ for various particle types relative to sea level flux. One can see from the table that non-muon fluxes are significantly affected in going from sea level to Fermilab altitude. Please note that the CRY-based particle rates shown in this document *do not include* this correction.

Particle type	L (gm/cm ²)	Sea Level flux	226 m	750 m
Neutrons	148	1	1.20	1.81
Protons	110	1	1.28	2.22
Electrons	100	1	1.31	2.41
Muons	520	1	1.05	1.18

Table 1: Table of relative increases with respect to sea level flux. Increase in flux is shown for Fermilab altitude (226 m) and 750 m. L is the absorption length in terms of atmospheric density assuming average barometric pressure and temperature of 0⁰ C. Any energy dependence of absorption processes is ignored.

CRY particle sampling is based on precomputed tables derived from a full MCNPX 2.5.0 [9] simulation which assumes *only* galactic protons in the incident flux spectrum. Figure 4 (left) shows the energy spectrum of galactic protons incident on Earth, only the highlighted region of the spectrum is used in the simulation. As will be seen from Section 4, the absence of non-proton nuclei in the incident flux severely underestimates the resulting hadron fluxes at all energies.

¹Estimating the relative increase in cosmic flux at 750 m is relevant to understand the effect introduced by a bug in the simulation software which will be discussed later in this section.

111 Another known problem in CRY is that it uses large bin widths to store energy spectra which results
 112 in inaccurate sampling of particle flux spectra. Figure 4 (right) shows the CRY generated energy spectra
 113 for μ^- and μ^+ and one can clearly see the step-like structure (especially after 40 GeV or so) caused due
 114 to large bin widths.
 115

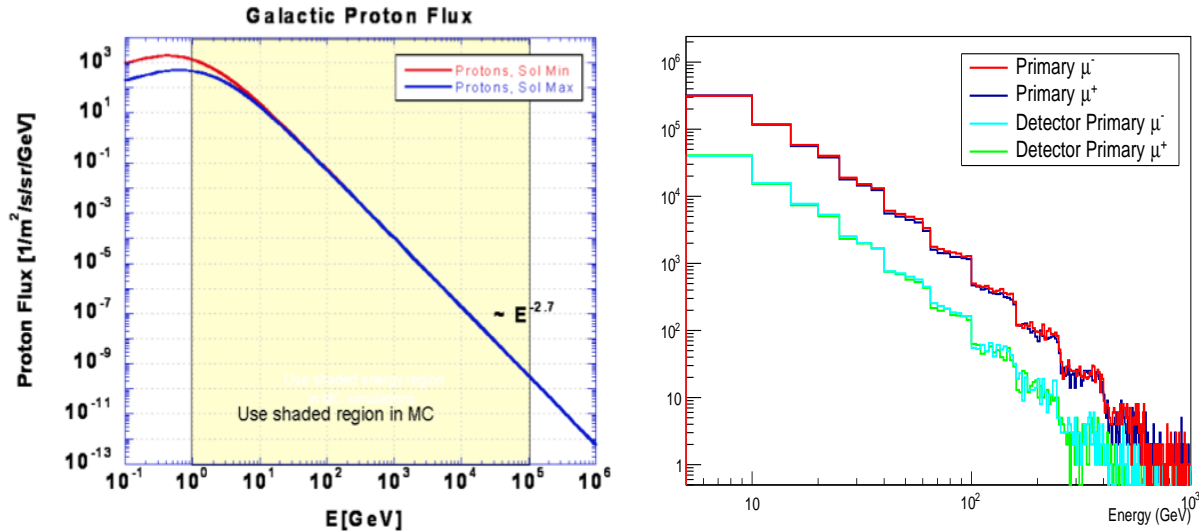


Figure 4: (Left) Energy spectrum of galactic protons incident on earth [1]. (Right) Muon energy spectra as generated by CRY.

116 3.1 CRY in LArSoft

117 For a given altitude, CRY generates particles on a square plane surface (referred to as *sub-box* in CRY
 118 jargon) of $n \times n$ meters size where n is specified by the user. The default location of the sub-box is
 119 the center of the detector. The maximum allowed value for sub-box length is 300 m. In MicroBooNE,
 120 the default value of n is set to 75 m, which is big enough to cover the diameter of the experimental
 121 hall (~ 15 m) and a good portion of the surroundings (~ 47 m). Next, the particles are projected back
 122 to the edge of the world volume². The current dimensions of world volume in Geant4 are set to be
 123 $1483 \times 1060 \times 1483$ m³. Finally, Geant4 propagates particles from the edge of the world box through
 124 the geometry, simulating particle interactions and decays during the propagation.

125
 126 CRY is interfaced into LArSoft in two stages. The first stage of integration is through *CRYHelper*,
 127 a class in *NuTools*. *CRYHelper* class configures CRY and performs the coordinate transformation into
 128 the MicroBooNE lab frame (in which the CRY generating surface is taken as ground level) and projects
 129 the particles to the surface of the world volume. The second CRY interface in LArSoft is the *Cosmic-*
 130 *sGen_module*, a class in the *larsim* repository that retrieves the output of *CRYHelper* and determines
 131 which particles to feed to Geant4. To be passed to Geant4, the point of closest approach (poCA) of the
 132 particle's straight-line trajectory to the center of the cryostat must be inside the cryostat-sized bounding
 133 box.

134
 135 A significant difference in primary muon rates between the CRY and Geant4 simulation steps [10]
 136 was observed. Ideally, one would expect these rates to be very close since muons are least affected by

²World volume here refers to the highest volume in the geometry which is adequately sized to include the detector enclosure and all important elements surrounding it.

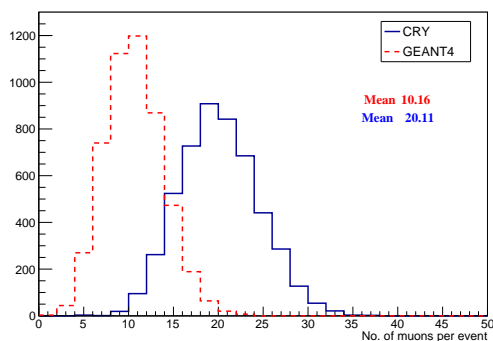


Figure 5: Distribution of number of muons entering the detector per 6.4 ms as simulated by CRY (solid blue line) and Geant4 (dashed red line).

137 the materials surrounding the detector. Figure 5 shows the distribution of number of muons entering
 138 the detector per 6.4 ms after CRY (solid blue line) and Geant4 (dashed red line) stages. From the
 139 figure, one can see that CRY and Geant4 predict on an average ~ 5 and ~ 2.5 muons per 1.6 ms
 140 time window, respectively. Almost 50% of the CRY-predicted muon flux is lost between the two simulation
 141 steps. The CRY-predicted muon flux is comparable to the measured (lower bound) rate of ~ 4 kHz (or
 142 6 muons per 1.6 ms time window) as reported by K. Woodruff and L. Kalousis [11, 12].

143

144 This big discrepancy between the CRY and Geant4 rates was mainly due to two reasons:

- 145 • The CRY filter (*CosmicsGen_module*) in LArSoft that chooses which particles are to be simulated
 146 by Geant4 was flawed resulting in an 8% loss of muon flux through the top surface of the TPC [13].
- 147 • Due to multiple scattering, energy loss and other effects, cosmic particles that do not initially point
 148 to the cryostat (or TPC) may intersect it after their trajectory is fully simulated with Geant4 (or,
 149 vice versa). So, a *buffer box* was added around the cryostat for increased acceptance at CRY-level
 150 and also to provide enough room for multiple scattering effects.

151 The next section gives details on validating the CRY interface in LArSoft and also compares the CRY-
 152 predicted primary muon flux against data after implementing solutions to the above problems.

153 3.2 CRY Muon flux validation

154 The first part of this section validates stand-alone CRY predictions for primary muon flux with measured
 155 flux. The second part of this Section validates the CRY interface in LArSoft. Ref. 16 provides two
 156 measurements of the muon flux through a horizontal surface [12]:

- 157 1. Ground level (Fermilab is at an elevation of 226 m above sea level): 141 ± 21 Hz/m²
- 158 2. Bottom of the experimental pit: 106 ± 16 Hz/m²

159 Using the stand-alone CRY installation in LArSoft, the CRY-predicted primary muon flux through a
 160 horizontal surface that is of the size of the top surface of the TPC is calculated to be 115 Hz/m². Ta-
 161 ble 2 compares measured rates with CRY-predicted rates with and without the correction for Fermilab's
 162 elevation. From the table, one can see that stand-alone CRY is reasonably consistent with measure-
 163 ment, although it might actually be slightly low given that the error bars on the measurement are very
 164 conservative.

165

Measured rate (Fermilab) (Hz/m ²)	Stand-alone CRY (sea-level) (Hz/m ²)	Stand-alone CRY (Fermilab) (Hz/m ²)
141±21	115	120.5

Table 2: Sea level flux through a horizontal surface that is of the size of the top surface of the TPC. This table compares measured rates to CRY-predicted rates. Last column shows the CRY-predicted flux corrected to account for Fermilab’s elevation.

Stand-alone CRY (Hz/m ²)	CRY+CRY Helper (Hz/m ²)	CRY+CRY Helper+ <i>CosmicsGen_module</i> (Hz/m ²)
115	115	106

Table 3: Sea level flux through a horizontal surface that is of the size of the top surface of the TPC. Table shows rates at each stage of the integration software.

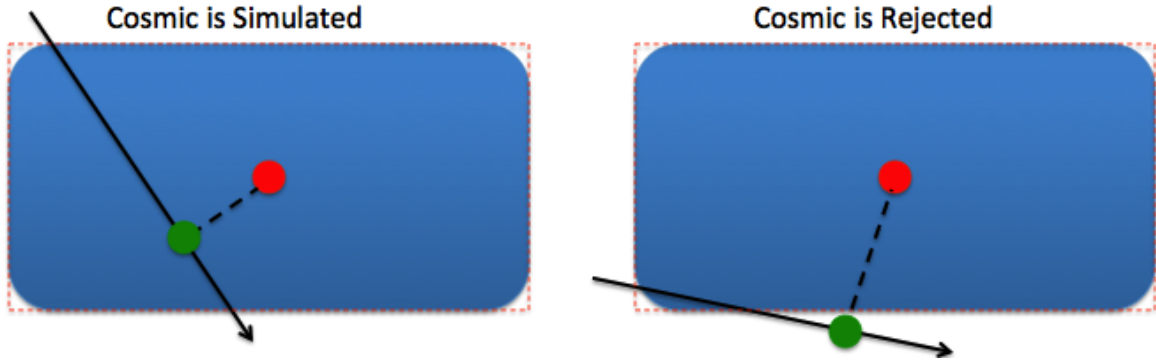


Figure 6: Given the non-spherical shape of the cryostat, this cartoon illustrates how the poCA of the particle can fall outside the cryostat even though it manages to cross the cryostat boundaries [13]. The black arrow represents the cosmic particle’s projected trajectory, the solid red dot represents the geometric center of the cryostat, the solid green dot represents the poCA to the center of the cryostat, and the dashed red box represents the cryostat boundary.

166 At each step of the CRY-LArSoft interface, primary muon flux through the top surface of the TPC
167 is calculated to validate the CRY interface in LArSoft. Table 3 shows the summary of primary muon
168 flux predictions at each step of the CRY-LArSoft integration. It is evident from the table that the
169 muon flux through the TPC surface is decreased due to the filtering scheme in the *CosmicsGen_module*.
170 The reason the flux decreases is because the cryostat-sized bounding box used in the simulation is not
171 spherical. So, it is possible for a particle to intersect the bounding box volume but its poCA to the
172 center of the volume could very well be outside the volume, as illustrated in Figure 6. This bug is fixed
173 by requiring the particle to intersect at least one of the cryostat bounding surfaces to be passed on to
174 the next simulation stage. After the bug fix, the primary muon flux is calculated to be 115 Hz/m²,
175 which matches the stand-alone CRY prediction. This fix is implemented in Larsoft version v03_07_00.

176
177 The *CosmicsGen_module* was also modified to include a user-configurable buffer box around the
178 cryostat (available from larsoft version v03_04_02). As mentioned in the previous section, the buffer box
179 increases the cosmogenic particle flux simulated in the detector by accepting particles that also enter
180 the detector due to multiple scattering effects. To determine an optimal size for the buffer box, a cosmic
181 sample with a very large buffer (10 m) region in all directions of the cryostat is generated to study the
182 maximum deflection points of particles that enter the TPC [14]. Figure 7 shows the maximum deflection

183 points of cosmic muons entering the TPC using a 10 m buffer box cosmic sample. One can see from
 184 the figure that while a lot of deflections happen close to the cryostat, some happen as far away as the
 185 ground level. The distribution of maximum deflection angles along muon's trajectory before it enters
 186 the TPC is shown in Figure 8 (left) and deflection angle of muons entering the TPC as a function of its
 187 energy at the largest scattering point is shown in Figure 8 (right). As expected, muons with low energy
 188 suffer large deflections.

189
 190 Based on the optimization studies [15], a 2.5 m buffer in each direction of the cryostat is recommended
 191 for MicroBooNE in order to regain the lost muon rate due to multiple scattering. Whenever a buffer
 192 box is specified by the user, the *CosmicsGen_module* checks for intersection of particles with the buffer
 193 box boundaries, rather than the cryostat boundaries. Note that the default simulation still uses a buffer
 194 box of zero size. Figure 9 shows muon rate (per 6.4 ms window) for CRY and Geant4 after the bug fix
 195 and considering a 2.5 m buffer box around the cryostat. It is evident from the figure that the two rates
 196 agree very well.

197 3.3 Other issues in cosmic simulation

198 As mentioned before, the CRY-LArSoft interface takes the cosmic particles generated at sea-level and
 199 projects them back to the world volume boundaries. This introduces an additional *absorption effect* due
 200 to the presence of atmosphere between the roof and the world volume boundaries. So, the CRY interface
 201 in LArSoft actually delivers a diminished flux corresponding to sea-level minus 530 meters (The top
 202 edge of the world volume boundary in the Y direction is at 530 m from the center of the TPC). Figure 10
 203 shows this absorption effect for muons and protons. In order to remove this additional absorption, an
 204 approximate solution³ is sought out by modifying the geometry simulation to fill the area between the
 205 roof and the top Y world volume boundary with vacuum (please note that this is only a partial solution
 206 since the particles can still decay along the ~ 500 m path). Table 4 shows how particle rates are in-
 207 creased when this additional absorption is partially removed with the proposed geometry modification.

³A more permanent solution to this problem would be to stop projecting particles to the world volume boundaries. The implementation of this fix is currently being worked on.

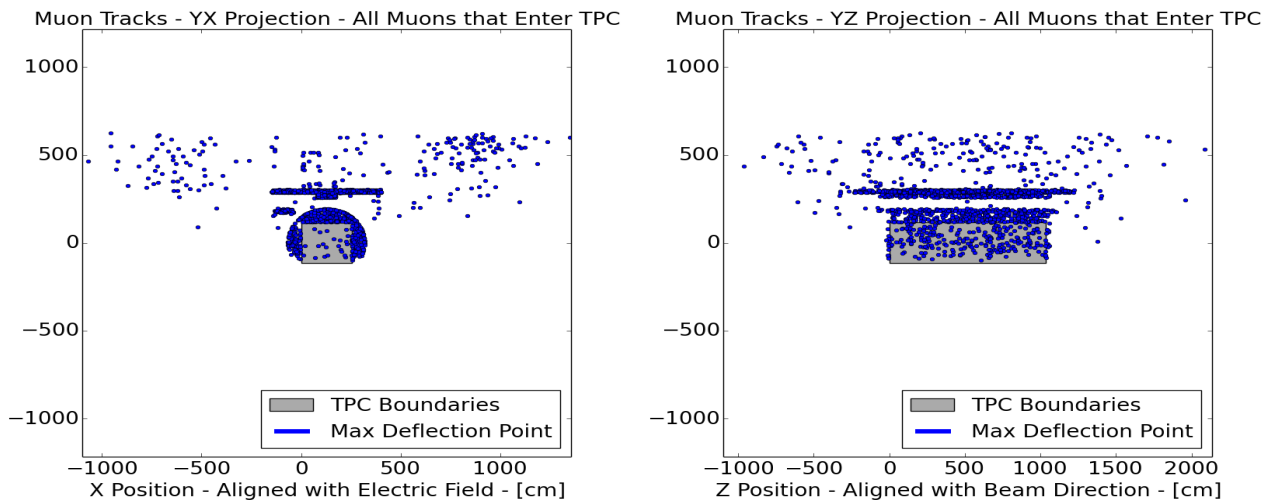


Figure 7: Position of largest deflection points of all cosmic muons that enter the detector in the YX projected plane (left) and YZ projected plane (right) of the MicroBooNE TPC. Plots are mainly shown for illustration using a cosmic sample of 90 events with 10 m buffer box [14].

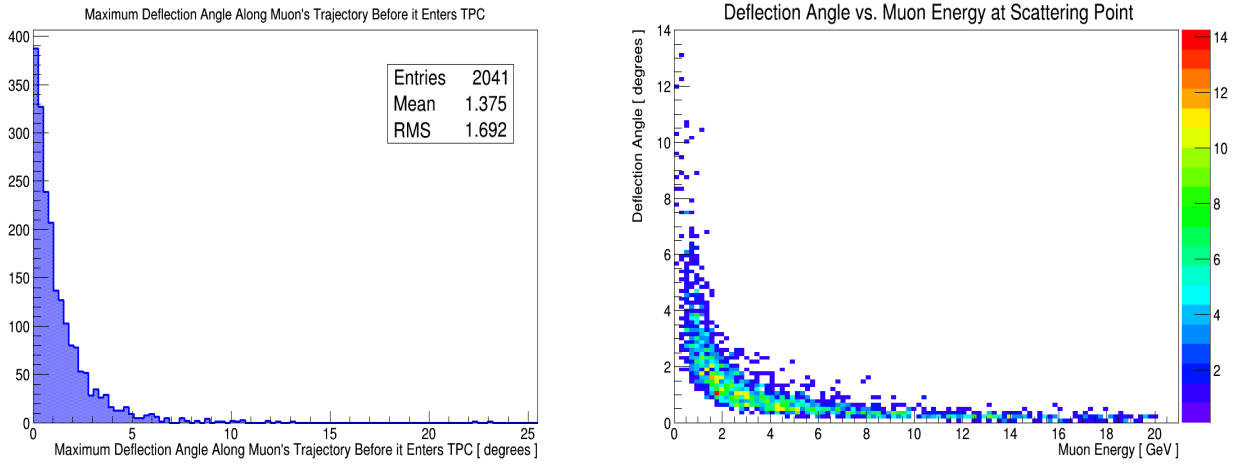


Figure 8: Distribution of maximum deflection angles along muon’s trajectory before it enters the TPC (left) and deflection angle of muons entering the detector as a function of their energy at the largest scattering point (right) [14].

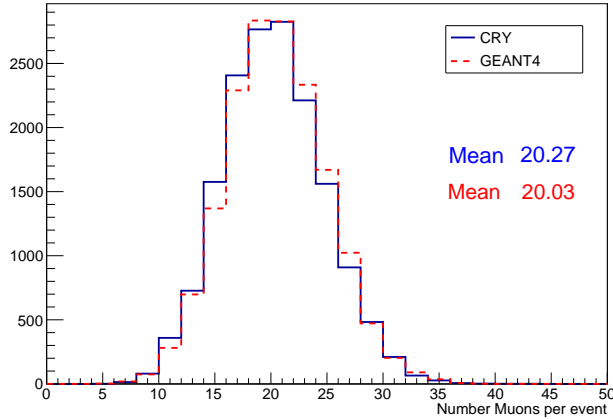


Figure 9: Distribution of number of muons per event as simulated by CRY (solid blue line) and Geant4 (dashed red line) using the improved CRY interface and a 2.5 m buffer box around the cryostat (compare to Figure 5). An event in this case corresponds to 6.4 ms time window.

208 As seen from the table, the 530 m additional absorption results in a $\sim 20\%$ loss of flux for muons. In the
 209 case of neutrons and protons the effect is huge resulting in fluxes that are diminished by ~ 2.5 to 3 times.
 210

211 Another issue observed in LArG4 (Geant4 interface in LArSoft) is that a lot of neutrons with
 212 significant energy start and end at the same Y position. In other words, LArG4 doesn’t seem to
 213 track these neutrons. This significantly affects both the CRY and CORSIKA simulated neutron rates.
 214 Figure 11 demonstrates this feature. These processes are identified as “nkiller” processes that kill
 215 neutrons after $10 \mu\text{s}$. The *NeutronTrackingCut* in the LArG4 physics list enables the neutron killer
 216 process. This issue was fixed by removing the neutron tracking cut from the configuration file. More
 217 details on this can be found in Appendix B. Using a CRY sample, Table 5 shows how the neutron and
 218 proton rates increase after removing this cut. One can see from the table that the neutron (and proton)
 219 rates almost double without the neutron tracking cut. Effect of this cut on CORSIKA samples and
 220 energy distributions of neutrons and protons for CRY and CORSIKA with and without this cut can be
 221 found in Appendix B.

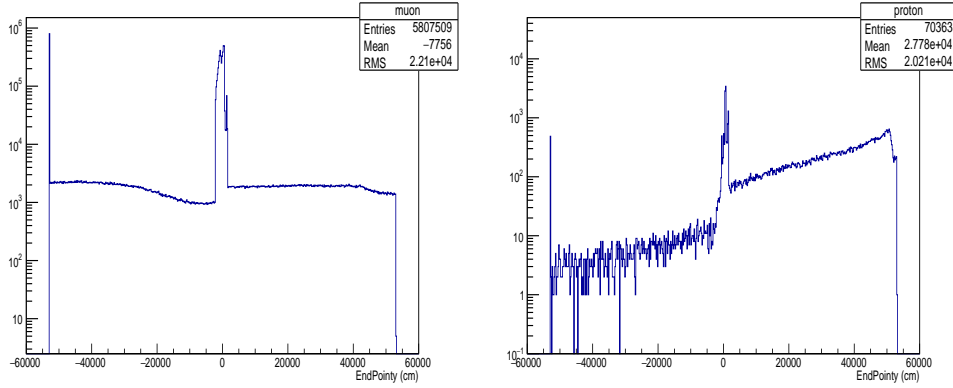


Figure 10: End point distribution of muons (left) and protons (right) in the Y-direction (in cm). Notice the absorption of particles happening between the building roof (18 m) and the top world volume boundary (530 m).

Particle type	World volume (Air)	World volume (Vacuum)	Ratio
μ^-	2.474 ± 0.004	2.932 ± 0.004	1.19
μ^+	2.559 ± 0.004	3.094 ± 0.004	1.21
neutron	0.815 ± 0.002	2.059 ± 0.004	2.53
proton	0.074 ± 0.001	0.201 ± 0.001	2.72
γ (>100 MeV)	0.435 ± 0.002	0.468 ± 0.002	1.08
e^- (>100 MeV)	0.838 ± 0.002	0.900 ± 0.002	1.07
e^+ (>100 MeV)	0.229 ± 0.001	0.255 ± 0.001	1.11

Table 4: Total number of particles expected in the TPC active volume per 1.6 ms time window for various particle types when the world volume is filled with air (column 2) and when it is filled with vacuum (column 3).

222 4 CORSIKA Cosmic ray simulations

223 The COsmic Ray Simulations for KAscade (CORSIKA) cosmic ray simulation package is used to validate
 224 and cross-check the cosmic ray particle fluxes predicted by CRY. CORSIKA allows for the study of

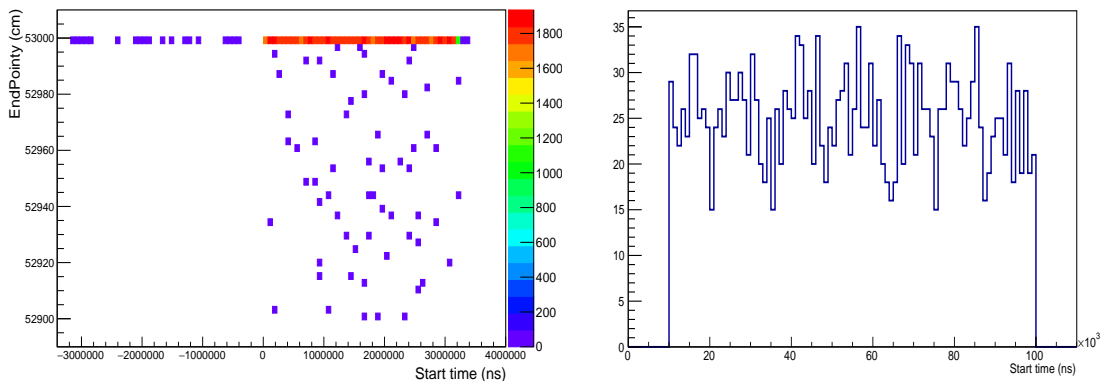


Figure 11: (Left) End points in the y-axis vs the start time for primary neutrons from CRY simulation. Notice that before $t=0$, not many neutrons end at their start y position (530 m), but, after $t=0$ many neutrons are killed immediately. (Right) Distribution of the start time of CRY generated primary neutrons that get killed right at their start Y point. Notice that this starts to happen after $10 \mu s$.

Particle type	with nkiller	without nkiller	Ratio
μ^-	2.933 ± 0.004	2.932 ± 0.004	1.00
μ^+	3.099 ± 0.004	3.094 ± 0.004	1.00
neutron	2.059 ± 0.004	4.099 ± 0.005	1.99
proton	0.201 ± 0.001	0.349 ± 0.001	1.40
γ (>100 MeV)	0.468 ± 0.002	0.468 ± 0.002	1.00
e^- (>100 MeV)	0.900 ± 0.002	0.899 ± 0.002	1.00
e^+ (>100 MeV)	0.254 ± 0.001	0.256 ± 0.001	1.04

Table 5: Total number of particles expected in the TPC active volume per 1.6 ms time window for various particle types with and without the nkiller process.

225 features not implemented in CRY, in particular:

- 226 • simulating multiple primary particle types beyond protons
- 227 • simulating the particle fluxes at the Fermilab elevation (226 m)
- 228 • testing alternate models for cosmic shower evolution (e.g. FLUKA)
- 229 • simulating cosmogenic particle fluxes below 50 MeV

230 By working with a NO ν A collaboration member [16], it was possible to quickly adapt CORSIKA output
 231 parsing and shower processing code to feed into LArSoft. A more detailed technote is being prepared
 232 that describes the steps required to run CORSIKA and process its output, and also contains detailed
 233 comparisons between CRY and CORSIKA predictions.

234 4.1 Running & Interfacing with CORSIKA

235 CORSIKA version 7.4003 is used to generate a large sample of showers for various primary particle
 236 types. In order to generate enough showers to cover one event, consisting of 6.4 ms or four readout
 237 frames, it was necessary to run roughly 800,000 proton showers. For the studies considered here, two
 238 events were generated per grid job submitted.

239 There are a large number of configurable options available in CORSIKA. A subset of these options
 240 was explored and, in particular, the primary particle type, primary low energy cutoff, and low-energy
 241 hadronic interaction model were varied. The primary types can be any element. In order to compare
 242 with CRY, protons were chosen as well as a combination of elements to implement a multi-component
 243 model that will be discussed below. The primary low energy cutoff controls the lowest energy per nu-
 244 cleon and is typically around 1 GeV. Below 1 GeV the resulting shower particles have a low probability
 245 of reaching the surface. The optimal value for this parameter depends on the altitude being considered.
 246 The low-energy hadronic interaction model is also configurable in CORSIKA. The two models studied
 247 are GHEISHA and FLUKA and will be discussed below.

249 The binary output from CORSIKA is processed using the *corsika converter* program, adapted from
 250 work done in the NO ν A collaboration [16]. This program parses the output of CORSIKA simulations
 251 into ROOT TTrees and also exports the particles into the *hepevt* format, allowing the particles to be
 252 fed into larsoft. The *corsika converter* program also arranges the particles, in time, into spills of du-
 253 ration specified during program compilation. The showers are arranged within a spill according to the
 254

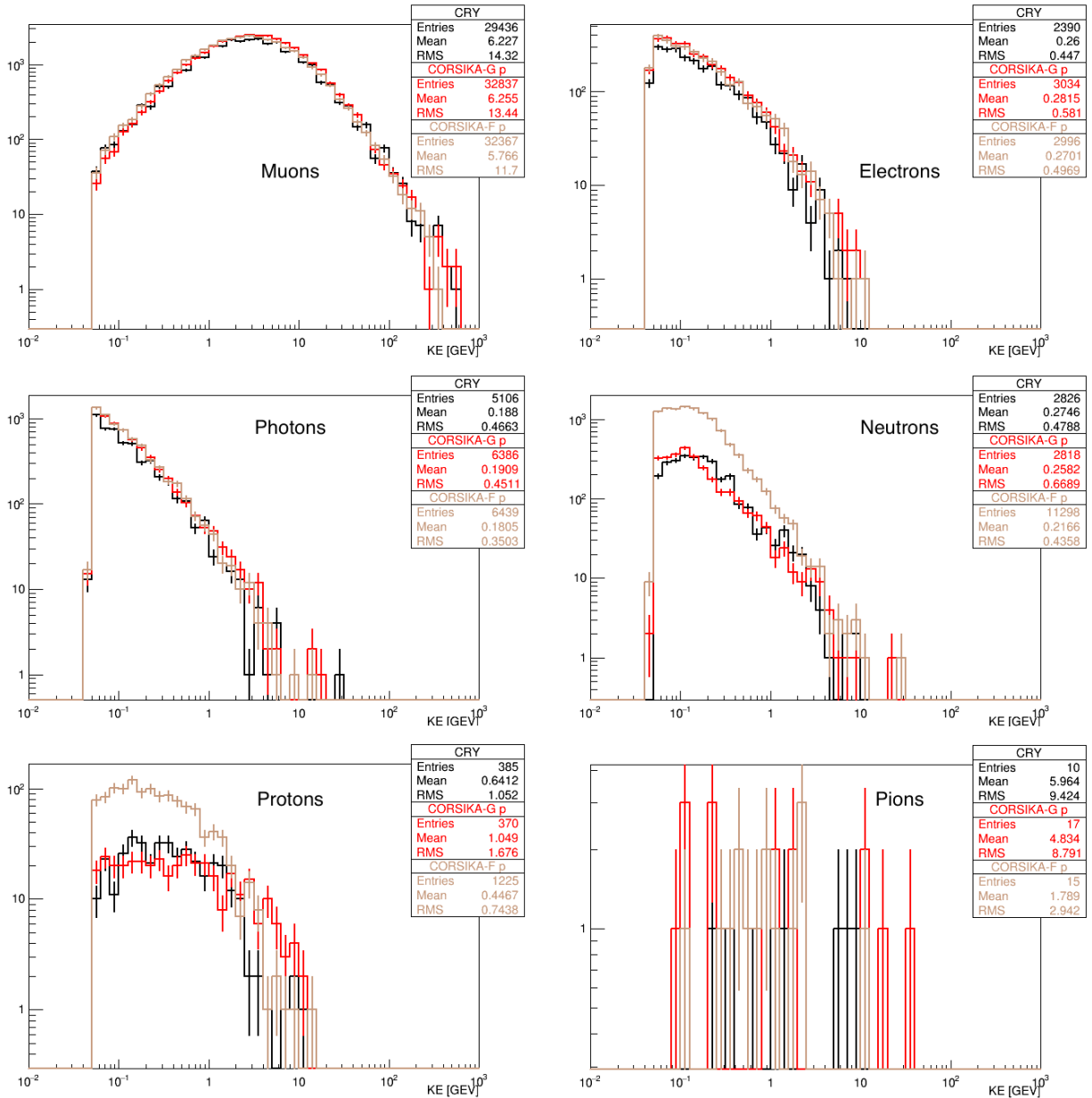


Figure 12: Comparisons of the energy distributions for each particle type through the top surface of the TPC active volume for CRY (black), CORSIKA-GHEISHA (red), and CORSIKA-FLUKA (tan). All three samples use only proton primaries and are made up of 2000 events that are 4.8 ms (3 read-out frames) long.

255 measured rate of proton primaries hitting the Earth's atmosphere. The particles are also arranged in
 256 space. The particles are distributed at the x, z position at which they reach the surface in the shower
 257 simulation. This area can be of the order of 100 square kilometers. In order to speed up the simulation
 258 it is optimal to distribute these particles over a horizontal box encompassing the top of the detector.
 259 By default, *corsika converter* program arranges the showers randomly in the x and z dimensions at a
 260 horizontal box placed at the top of the detector. In order to preserve any spatial correlations that may
 261 exist among the particles in the shower, this part was modified to wrap the particles in space, so that
 262 for example, a particle starting just beyond the +z edge of the horizontal box, would be wrapped to
 263 start just inside of the -z edge.

265 The spill duration is chosen to encompass four readout frames, or 6.4 ms, matching CRY. The area
 266 chosen for the horizontal box was 10 m beyond each side of the top of the TPC in the x and z dimensions,
 267 685 m². With these parameters chosen for the CORSIKA simulation, a 6.4 ms spill duration can be
 268 filled with approximately 1.6 million proton primary showers distributed between 1.4 GeV and 100 TeV.

269 4.2 Flux Comparisons between CORSIKA and CRY

270 The dominant uncertainty in computing cosmogenic fluxes comes from the particle interaction models
 271 so it is important to consider the effects of model choices on the resulting secondary particle fluxes. As
 272 stated above, the neutron fluxes predicted by CRY are known to be too low when compared with data.
 273 Experimental data from BESS [18], indicates that FLUKA does a better job of modeling hadronic
 274 interactions at low energy, particularly for protons. CORSIKA can use the FLUKA 2011 model for
 275 hadronic interactions below 80 GeV, but, by default, GHEISHA is used and is built into the CORSIKA
 276 distribution. CORSIKA has to be pointed to the location of a working FLUKA installation in order to
 277 use the FLUKA model.

278

279 Figure 12 shows comparisons of the flux, for each simulated particle type, between CRY and COR-
 280 SIKA with the GHEISHA or FLUKA model used for low energy hadronic interactions. The fluxes
 281 coming from CRY and CORSIKA with the GHEISHA model are similar, but CORSIKA predicts a
 282 significant increase in the electromagnetic component. The wide energy bins in CRY can also be seen,
 283 for example, in the photon energy spectrum and the continuous energy spectra coming from CORSIKA
 284 do not exhibit the same steps.

285

286 In changing from the GHEISHA model to the FLUKA model the fluxes of muons, electrons, photons
 287 remain essentially unchanged. The neutron and proton flux, particularly below 1 GeV, is increased
 288 dramatically. The integrated neutron flux increases by a factor of 4.0 while the proton flux increases by
 289 a factor of 3.3.

290 4.3 The CMC Model

To account for primary types beyond just protons and the resulting cosmic ray showers it is necessary
 to simulate the various primary types entering the atmosphere. Simulating all primary types would be
 computationally prohibitive so it is ideal to use a parametrization that reproduces the spectrum from
 a full range of primary types using only a subset of the possible primary types. The Constant-Mass
 Composition (CMC) model [17] does just this using five components with a constant spectral index
 between each primary type. The CMC model models the primary flux using protons, He, N, Mg, and
 Fe. The flux of each primary type is specified via:

$$\Phi_A(E) = K_A(E/1 \text{ GeV})^{-\gamma_A}$$

291 where A is the index of the primary type, E is the energy of the primary particle (per nucleon), K_A is
 292 the flux constant for primary type A, and γ_A is the spectral index of primary type A. Table 6 lists the
 293 flux constant and spectral index for each primary type.

294 In order to implement the CMC model within the CORSIKA framework it was necessary to run a
 295 sufficient number of showers of each primary type with the specified spectral index. The showers were
 296 then arranged into spills with the duration of 4 readout frames (6.4 ms) at the surface based on the
 297 specified flux constant for each primary type. The resulting lists of particles were then concatenated to

298 form the total CMC model cosmogenic particle flux.

299

300 Figure 13 shows CRY and CORSIKA-FLUKA cosmogenic particle flux predictions at the top of the
 301 MicroBooNE TPC. CORSIKA predictions are provided for both the proton-only and CMC primary
 302 models. In general the change from the proton only model to the CMC model increases the flux of each
 303 type of cosmogenic particle. Table 7 gives the expected rate for each particle type along with the ratio
 304 of the rate relative to the CRY rate. The muon rate increases drastically, by 40%, when considering the
 305 CMC model. The neutron rates increase by a factor of 5. Note that for the rest of this note, CORSIKA
 306 with CMC and FLUKA configuration represents our nominal simulation and all conclusions are derived
 307 based on this sample.

308 5 Analysis framework and data samples

309 All the studies shown in this document are done at truth level (CRY and Geant4 [3]) using the Micro-
 310 BooNE specific AnalysisTree ntuples [4, 5]. AnalysisTree ntuples are flat ROOT ntuples obtained by
 311 a straight-forward unfolding of information available in an ART [7] event record.

312

313 The CRY and CORSIKA MC samples with and without overburden simulation are generated in
 314 LArSoft [6] version v04_14_00 which incorporates all the bug fixes discussed in Section 3. Details about
 315 the overburden geometry can be found in Section 2. Each of the CRY samples is generated for $\sim 40,000$
 316 events. Event here corresponds to a total generation time of 6.4 ms (3.2 ms before trigger and after the
 317 trigger; trigger here represents the start of the drift window that encloses the beam gate). This broad
 318 generation time per event is required to accommodate cosmic tracks that occur at random times. With
 319 $\sim 40k$ events, each of the CRY generated samples correspond to 256 seconds in real time. Similarly,
 320 CORSIKA samples are generated for $\sim 20,000$ events (or equivalently 128 seconds in real time).

321

Primary	K	γ
p	1.72×10^4	2.71
α	9.20×10^3	2.71
CNO	6.20×10^3	2.71
Mg	9.20×10^3	2.71
Fe	6.20×10^3	2.71

Table 6: Flux constants (K) and spectral indices (γ) for each primary type in the CMC model [17].

Particle	CRY Rate	CORSIKA GHEISHA Proton		CORSIKA FLUKA Proton		CORSIKA FLUKA CMC	
		Rate	Ratio	Rate	Ratio	Rate	Ratio
μ^\pm	114.3 ± 0.2	128.7 ± 0.7	1.12 ± 0.01	127.7 ± 0.2	1.117 ± 0.003	160.9 ± 0.3	1.407 ± 0.003
e^\pm	9.5 ± 0.1	11.9 ± 0.2	1.27 ± 0.03	11.8 ± 0.1	1.24 ± 0.01	14.7 ± 0.1	1.55 ± 0.01
γ	19.7 ± 0.1	25.0 ± 0.3	1.25 ± 0.02	25.1 ± 0.1	1.27 ± 0.01	31.3 ± 0.1	1.59 ± 0.01
n	11.1 ± 0.1	11.0 ± 0.2	1.00 ± 0.03	44.6 ± 0.1	4.02 ± 0.03	56.6 ± 0.1	5.10 ± 0.03
p	1.5 ± 0.02	1.4 ± 0.1	0.96 ± 0.1	4.8 ± 0.04	3.19 ± 0.06	6.0 ± 0.1	3.96 ± 0.07
π^\pm	0.023 ± 0.003	0.067 ± 0.02	1.7 ± 0.7	0.045 ± 0.004	2.0 ± 0.3	0.059 ± 0.005	2.6 ± 0.4

Table 7: Table of rates, in $\text{Hz} \cdot \text{m}^{-2}$, for CRY and the various CORSIKA configurations. Ratios are given relative to the CRY rate. The CRY rates are at sea-level while the CORSIKA rates are given at the Fermilab elevation. These are generator level rates and so do not include propagation/decay effects that would come from GEANT4.

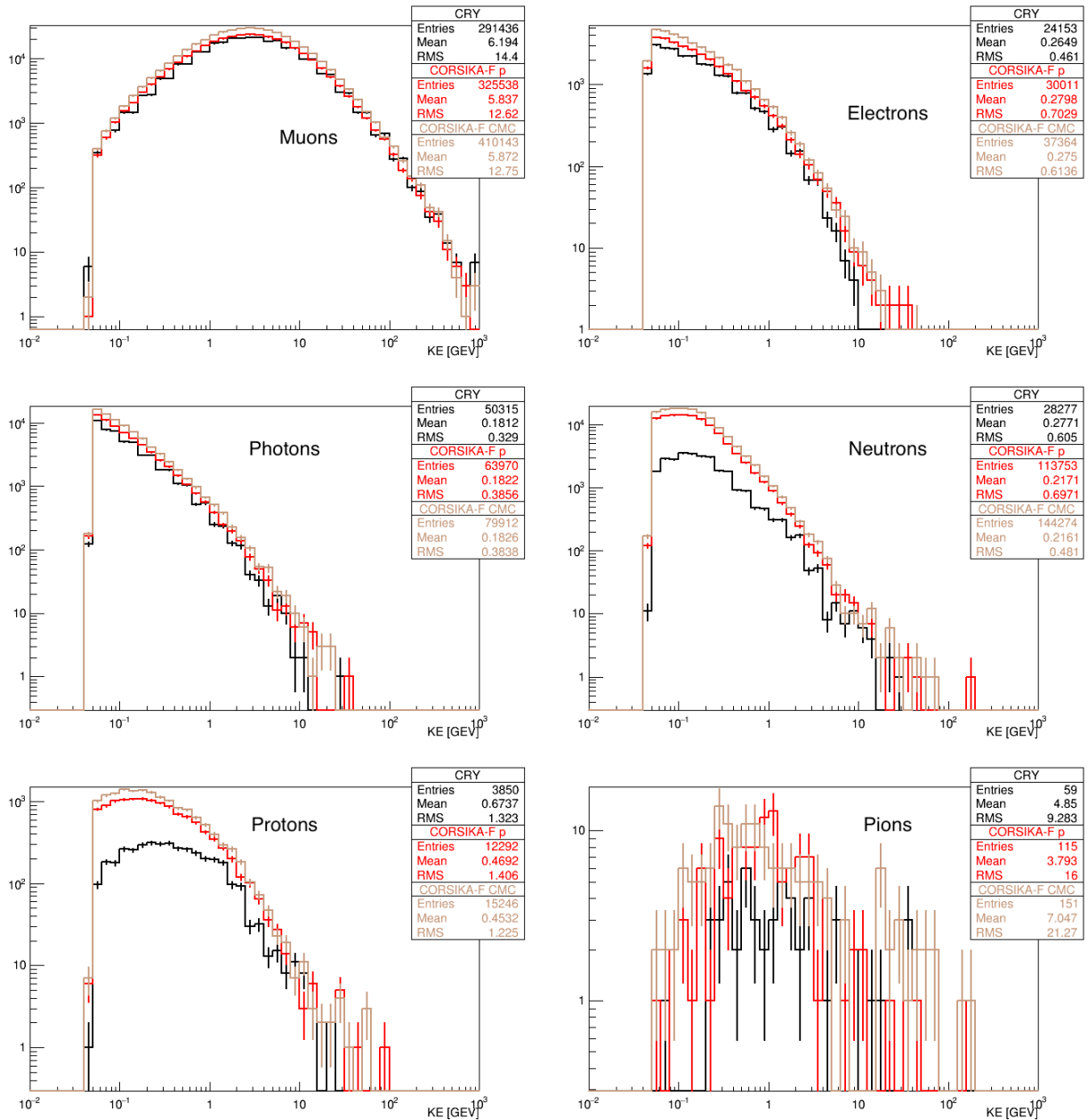


Figure 13: Comparisons of the energy distributions for each particle type through the top of the TPC active volume for CRY (black), CORSIKA-FLUKA with protons (red), and CORSIKA-FLUKA with the CMC Model (tan). The samples are made up of 19,982 events that are 4.8 ms (3 read-out frames) long.

322 In MicroBooNE, the total read-out time for a given event is three times the drift window at 500 V/cm
 323 ($3 \times 1.6 \text{ms} = 4.8 \text{ms}$ or equivalently 9600 time ticks with a sampling rate of 500 ns per tick). Although
 324 we are primarily interested in what happens in the drift window (1.6 ms), it is important to record
 325 information 1.6 ms preceding an event and 3.2 ms following an event in order to accommodate cosmic
 326 ray tracks that occur *during* an event drift time.

327
 328 At many places in the following sections, the event rates are quoted for 211 seconds or equivalently
 329 $1.32 \text{E}8$ beam spills (a beam spill window corresponds to 1.6 micro-seconds). The significance of 211
 330 seconds is that it corresponds to the total beam exposure time for a three year BNB run (or $6.6 \text{E}20$

331 POT) considering only beam coincident events. This is not realistic because it assumes 100% rejection
 332 of out-of-spill events, but does indicate the minimum background expected in a three year BNB run.

333 6 Simulated particle rates

334 This section presents estimates of the sizes of various backgrounds that enter the detector using CRY
 335 and CORSIKA cosmic samples without an overburden present. Table 8 shows the total number of
 336 cosmic particles that enter the TPC active volume in a 1.6 ms time window. As mentioned in Section
 337 4, even though the CORSIKA sample with CMC and FLUKA models represents the nominal simu-
 338 lation, for comparison estimates from CRY and other CORSIKA configurations are also shown. All
 339 CORSIKA numbers correspond to Fermilab elevation. CRY numbers correspond to sea-level; the rates
 340 will be higher if one takes into account Fermilab’s elevation above the mean sea level (refer to Table 1
 341 in Section 3). In addition to this, as discussed in Section 3, all CRY numbers suffer undercounting due
 342 to absence of non-proton primaries in the incident spectra⁴.

343
 344 Table 8 shows that muons and neutrons make up the majority of the background. The relatively
 345 high rate of neutrons⁵ is especially concerning. An energy cut of 100 MeV is placed on electrons and
 346 photons in order to not include the vast number of very low-energy particles which are of little interest
 347 for this study.

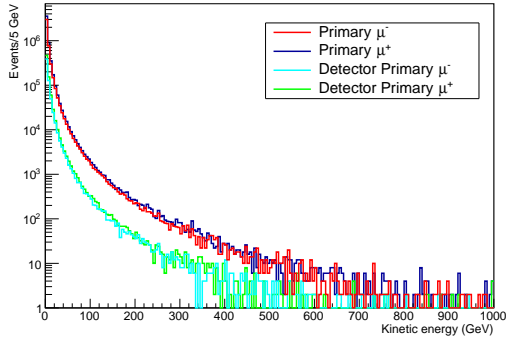
Particle type	CRY PROTON	CORSIKA CMC GHEISHA	CORSIKA PROTON FLUKA	CORSIKA CMC FLUKA
μ^-	2.932±0.004	4.22±0.02	3.093±0.006	4.006±0.007
μ^+	3.094±0.004	4.91±0.02	3.895±0.007	4.810±0.008
neutron	4.099±0.005	5.99±0.03	10.75±0.01	13.77±0.01
proton	0.349±0.001	0.54±0.01	0.969±0.004	1.245±0.004
γ (>100 MeV)	0.468±0.002	0.71±0.01	0.524±0.003	0.657±0.003
e^- (>100 MeV)	0.899±0.002	1.36±0.01	1.004±0.004	1.260±0.004
e^+ (>100 MeV)	0.256±0.001	0.37±0.01	0.280±0.002	0.347±0.002

Table 8: Number of primary plus secondary particles expected in the TPC active volume per 1.6 ms time window for various particle types. In this case, the geometry simulation doesn’t include any type of overburden. CRY numbers correspond to sea-level while CORSIKA numbers correspond to Fermilab altitude. In both cases the neutron killer process (refer to Appendix B) is turned off.

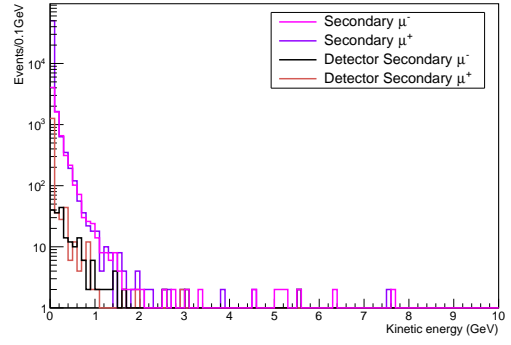
348 Figure 14 shows the kinetic energy distribution of important cosmic backgrounds predicted by the
 349 nominal simulation (CORSIKA with CMC and FLUKA models). As expected, most of the primary
 350 muons reach the detector and there is not much secondary muon production (Figures 14a and 14b).
 351 A large number of primary neutrons with kinetic energies between 0.1 and 4 GeV manage to reach
 352 the detector (see Fig. 14c). A lot of secondary neutrons are produced due to interactions of primary
 353 particles within and outside the detector as shown in Figure 14d. Although small compared to neutrons,
 354 the primary proton background rate is significant (Fig. 14c) and the secondary proton production is

⁴Note that all CRY numbers also suffer from the extra decays that occur as particles travel from the world volume edges towards the detector, although this effect is expected to be relatively small.

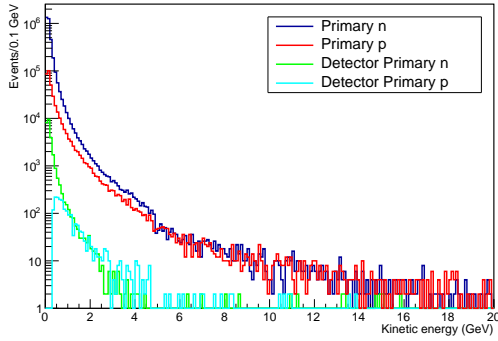
⁵Note that the total neutron/proton rate quoted in Table 8 (and Table 12) doesn’t take in to account the fact that Geant4 often gives new track IDs to particles that scatter. We estimated the effect of this Geant4 feature on the computed secondary rates by identifying all scattered tracks that get a distinct track ID from Geant4 than the initial main track and counting them as one track. More details on this can be found in Appendix A.



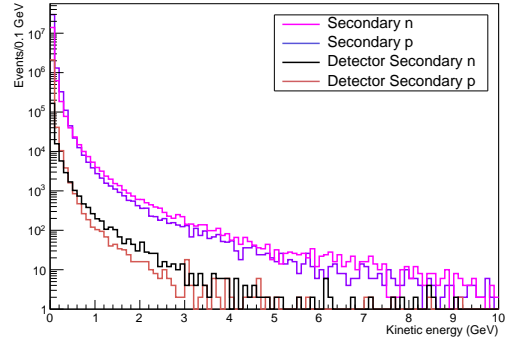
(a) Primary muons



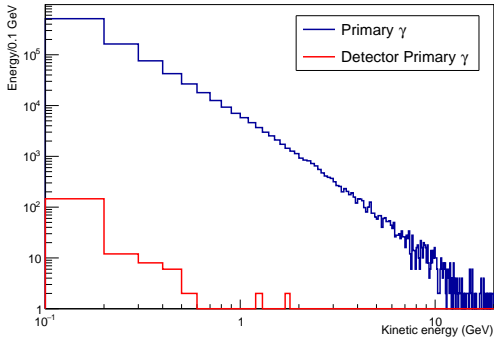
(b) Secondary muons



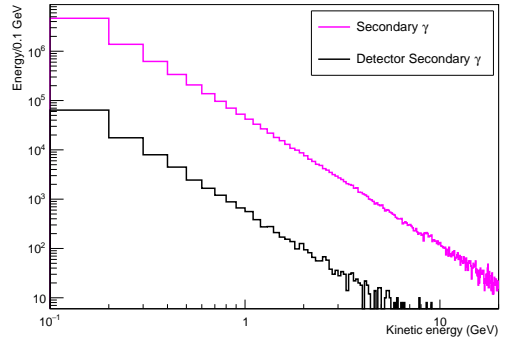
(c) Primary neutrons and protons



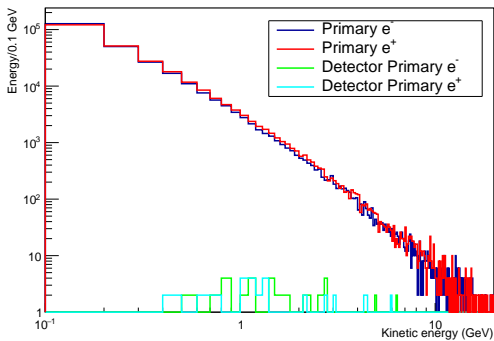
(d) Secondary neutrons and protons



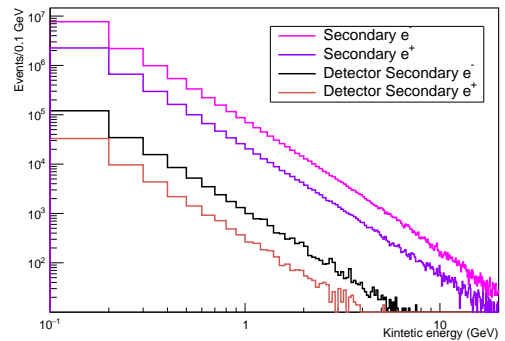
(e) primary photons



(f) secondary photons



(g) Primary electrons



(h) Secondary electrons

Figure 14: Kinetic energy distributions of various cosmic particles using the nominal CORSIKA sample without any overburden simulation. Plots also show the kinetic energy distributions of particles that enter the TPC active volume (referred to as “detector primary” or “detector secondary” in the plots). The photon and electron plots include an energy cut of 100 MeV. These plots are made using 40k events where each event corresponds to 6.4 ms of generation time (corresponds to a total of 256 seconds in real time). Please note the difference in axes scales between the plots.

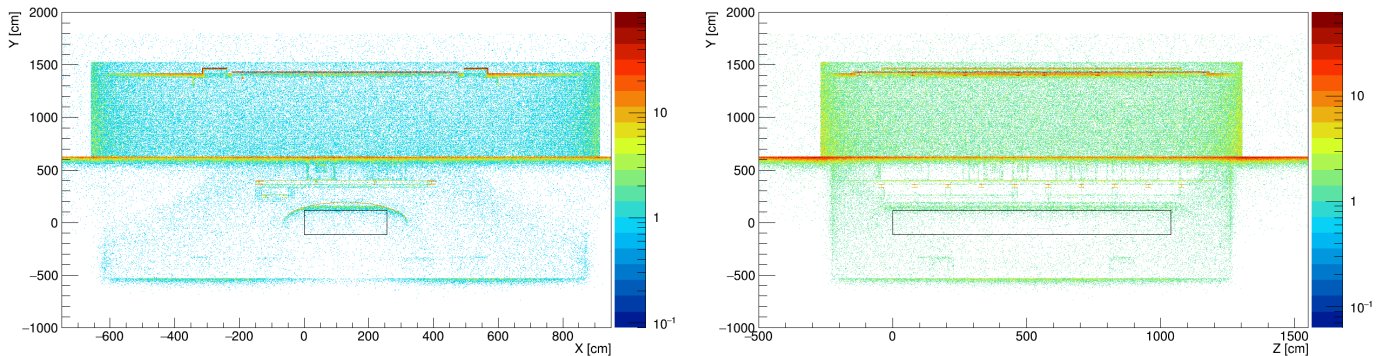


Figure 15: End point distribution of primary photons with energies above 100 MeV in the YX (left) and YZ (right) projection of the MicroBooNE TPC. The end point for photons is defined as the point where it converts. These distributions are obtained using a cosmic data sample with no overburden simulation.

355 comparable to neutrons (Fig. 14d).

356

357 It is interesting to note from Figures 14e and 14g that a small (but significant) number of primary
 358 photons and a negligible number of primary electrons/positrons with energies greater than 100 MeV
 359 reach the detector. This lower rate is due to the large amount of absorptive material surrounding the
 360 detector, including the inactive argon in the cryostat. Figure 15 shows how the primary photons are
 361 stopped in the surrounding volume of the TPC, especially in the liquid argon volume that surrounds
 362 the detector. This is due to the low radiation length of photons in liquid argon (~ 14 cm).

363

364 The secondary electron and photon backgrounds as shown in Figures 14f and 14h are mainly produced
 365 by muons through δ rays. It is this background that is worrisome for single e/γ searches. Also worrisome
 366 are the e/γ backgrounds induced by primary hadrons. The next part of this section shows a detailed
 367 study of these backgrounds.

368 6.1 Cosmogenic ν_e -like backgrounds

369 Cosmic events that induce EM showers inside the active volume of the detector can form a significant
 370 background to ν_e appearance searches. This background is mainly induced by primary muons that
 371 enter the detector volume or pass close to the walls of the detector. In this note, cosmogenic ν_e -like
 372 backgrounds are defined as follows:

- 373 • electrons created by a Compton scatter
- 374 • an e^+/e^- pair created by the photon pair production process

375 The two main physics processes that produce the parent photon of these backgrounds are the following:

- 376 • Primary muon produces a δ ray which creates a photon through bremsstrahlung. This is the
 377 dominant process.
- 378 • Primary muon creates a photon through bremsstrahlung directly. This process results in about
 379 3% of total events.

380 In addition to the above two processes, a high energy primary photon that passes close to the detec-
 381 tor walls can induce an EM shower. This rate is found to be non-negligible. The ν_e -like background is

Process	CRY PROTON	CORSIKA CMC GHEISHA	CORSIKA PROTON FLUKA	CORSIKA CMC FLUKA
Compton in spill, primary μ in AV	190 \pm 11	297 \pm 70	249 \pm 20	318 \pm 23
Pair production in spill, primary μ in AV	12220 \pm 90	18225 \pm 549	13369 \pm 150	15917 \pm 162
Compton in spill, primary μ not in AV	4	0	0	3
Pair production in spill, primary μ not in AV	144 \pm 10	33 \pm 23	29 \pm 7	71 \pm 11
Compton or pair production in spill, Primary is a γ	112 \pm 9	264 \pm 66	221 \pm 19	234 \pm 20
Pair production or Compton in spill, primary is not a μ or γ	652 \pm 21	1568 \pm 161	1238 \pm 46	1502 \pm 50
Charged current ν_e intrinsic [19]	~300-400			
Low energy excess signal events [20]	~100			

Table 9: Cosmogenic ν_e -like background rates ($E > 200$ MeV), without overburden simulation, occurring in the detector fiducial volume. The fiducial volume is defined as 30 cm upstream and 100 cm downstream in the beam direction and 25 cm from all other walls of the TPC. AV stands for active volume of the detector. For convenience, rates are shown for 1.32E12 beam spills which corresponds to 3 years of BNB run. An estimation of the signal events are also shown for comparison in the last two rows. The numbers in the last column represent our nominal sample; others are shown for comparison.

Process	CORSIKA CMC GHEISHA	CORSIKA CMC FLUKA
Compton in spill, primary μ in AV	1337 \pm 149	1401 \pm 48
Pair production in spill, primary μ in AV	46669 \pm 878	40645 \pm 260
Compton in spill, primary μ not in AV	0	5
Pair production in spill, primary μ not in AV	149 \pm 50	192 \pm 18
Compton or pair production in spill, Primary is a γ	908 \pm 122	816 \pm 37
Pair production or Compton in spill, primary is not a μ or γ	3698 \pm 247	3539 \pm 77

Table 10: Cosmogenic ν_e -like background showers with $E > 100$ MeV. Same description as Table 9 holds except for the energy cut.

382 also produced in significant quantities by other primary particles, such as neutrons, protons, and pions.
383 Table 9 shows ν_e -like background event rates expected from a three year BNB run corresponding to
384 a total POT of 6.6E20. Rates shown in the table require that the photon interaction which initiates
385 the EM shower occur in the fiducial volume of the detector, defined as 30 cm upstream and 100 cm
386 downstream in the Z direction (long direction, collinear with the beam) and 25 cm from all other walls of
387 the TPC. Also the photon energy must be greater than 200 MeV before the interaction. In a Compton
388 scatter, it is additionally required that the daughter electron has an energy greater than 200 MeV (for
389 comparison, Table 10 shows the background rates in which these energy cuts are 100 MeV). As can be
390 seen from the tables, the largest background comes from muon induced photons converting to e^+/e^-
391 pairs.

392
393 The listed backgrounds in Table 9 are sub-divided according to each photon's matching primary
394 particle. If the primary particle is a muon, a distinction is made as to whether it intersects the TPC
395 active volume boundaries or not. Classifying backgrounds this way provides crucial information for
396 applying cuts to reduce these background events. Figure 16 (left) shows the energy distribution of
397 ν_e -like background events as shown in Table 9. One can see from the figure that the energy of these
398 background events lie in the region of interest of MicroBooNE physics. An overburden will have little
399 effect on the rate of primary muons, the majority of which will enter the detector and act as primary
400 source of ν_e -like backgrounds. So, it is very important to devise a set of cuts to reduce this background
401 in order to successfully perform searches involving single electrons or photons.

402
403 A lot of studies recently took place in MicroBooNE to mitigate these backgrounds [21]. One of
404 the important cuts devised to reduce the muon induced shower background is the *muon cylinder cut*
405 which identifies and removes background showers that are close to a muon track. Non-muon induced

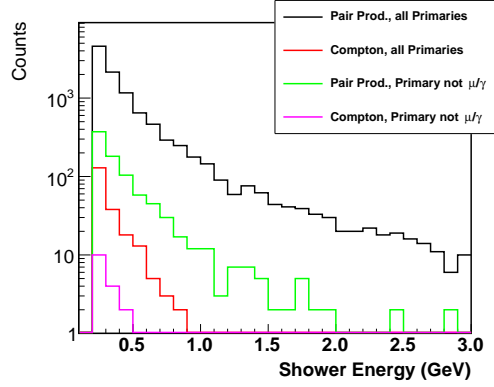


Figure 16: (Left) Energy distribution of cosmogenic ν_e -like background showers occurring in the detector fiducial volume (defined in the text) using the CORSIKA-CMC-FLUKA sample (without overburden simulation). Event rate corresponds to $6.6E20$ POT or equivalently $1.32E12$ beam spills. Red (black) line shows Compton (pair-production) background induced by primary muons and photons. Green and magenta lines show Compton and pair-produced background induced by non-muon or non-photon primaries.

Ancestor particle type	No. of particles
\bar{p}	37
π^-	111
e^+	34
e^-	50
π^+	83
p	413
n	178

Table 11: PDG codes of non-muon or non-photon primaries that are ancestors of a ν_e -like background shower (corresponds to row 6 in Table 9).

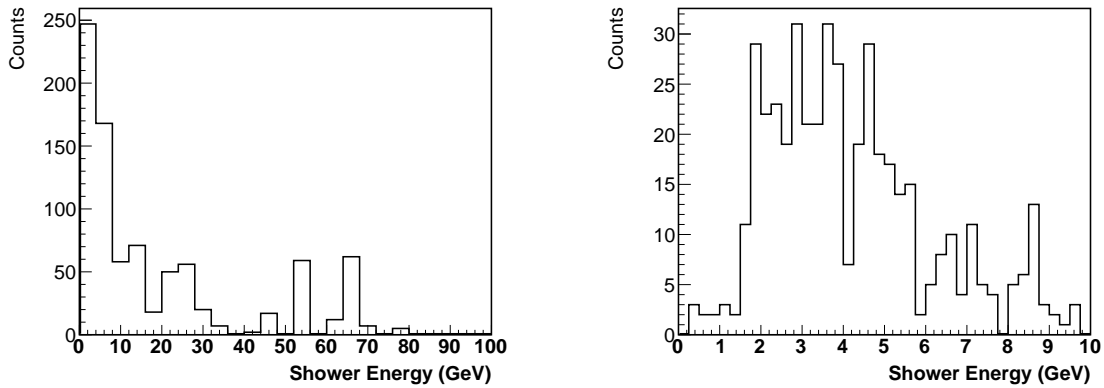


Figure 17: (Left) Number of ν_e -like background showers as a function of the energy of their matching non-muon or non-photon ancestor. Notice the really high energy ancestors that can result in a large number of showers. (Right) Zoomed in view of the plot on the left for the energy range 0 to 10 GeV.

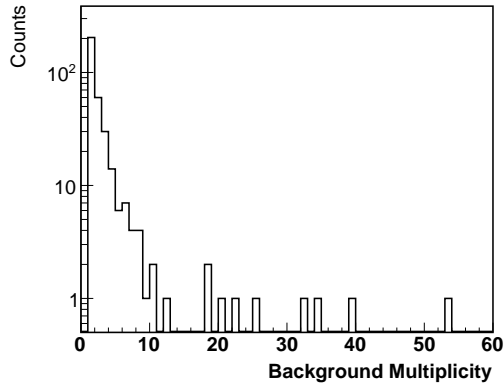


Figure 18: Shower multiplicity for non-muon and non-photon primaries.

406 showers (which are mostly pair-produced) are more challenging to remove; a combination of dE/dx and
 407 other cuts like backward distance to wall (BDtoW) or backward distance to top wall (BDtoTopW) are
 408 devised to reduce this background. Although the mitigation studies demonstrated good cosmic shower
 409 rejection efficiency, one cannot completely rely on them since they are performed with truth information
 410 and assume a flat 94% efficiency in identifying pair-produced showers. Also, the shower reconstruction
 411 efficiency is marginal below 200 MeV.

412
 413 In the case of non-muon and non-photon induced ν_e -like background (see row 6 of Table 9), the
 414 mechanism through which showers are created is usually a hadronic interaction that creates a neutral
 415 pion which then decays into a photon creating showers. Table 11 shows the PDG distribution of non-
 416 muon or non-photon primaries that are ancestors of a ν_e -like background shower. From the table, one
 417 can see that primary protons and neutrons contribute much more than other primaries in creating these
 418 ν_e -like backgrounds. Figure 17 shows the number of ν_e -like background showers as a function of the
 419 energy of their matching non-muon or non-photon ancestor. It is interesting to note that some of these
 420 hadronic showers create multiple background showers⁶ in the same event, see Figure 18. Comparing
 421 this background (rows 5 and 6 of Table 9) to the signal (rows 7 and 8 of Table 9), one can see that the
 422 non-muon induced background is several times larger than the signal.

423 7 The effect of an overburden

424 In this section, the effect of a three meter concrete overburden on various particle rates is shown. The
 425 overburden is located on the LArTF roof as a solid concrete disc with a diameter matching the ex-
 426 perimental pit. Given the position of the overburden in the MicroBooNE geometry, an overburden
 427 will *primarily* reduce the primary (or atmospheric) particle rates (some particles back scatter from the
 428 geometry below and enter the volume of the overburden but this rate is found to have no effect on
 429 the final results). Additionally, muons are mostly unaffected by concrete, so the primary motivation
 430 to install an overburden is to reduce the non-muon primaries, especially neutrons and electromagnetic
 431 backgrounds. The original motivation for the overburden was to remove ν_e -like backgrounds induced by
 432 primary cosmogenic photons. But, as seen in Section 6 (Fig. 14) and will be seen later in this section,
 433 the main source of ν_e -like background actually comes from primary hadrons, not photons.

⁶Such large energy depositions in the detector and multiple showers pointing to the same origin should provide an easily identifiable background signature and could probably be removed.

Particle type	Primary Particle rate		diff. (σ)	Secondary Particle rate		diff. (σ)
	(w/o OB)	(with OB)		(w/o OB)	(with OB)	
μ^-	528154±935	478276±890	-38.6	169±17	60±10	-5.6
μ^+	633114±1024	573600±975	-42.1	1176±44	267±21	-18.6
neutron	21879±190	5277±94	-78.3	1793492±1724	676482±1059	-552.2
proton	1581±51	129±15	-27.3	162642±519	45747±275	-198.9
γ (>100 MeV)	147±16	28±7	-7.0	86527±379	77256±358	-17.8
e^- (>100 MeV)	33±7	0	—	166126±525	150753±500	-21.2
e^+ (>100 MeV)	27±7	0	—	45780±275	38403±252	-19.8

Table 12: Primary and secondary particle rates expected in the TPC active volume for various particle types with and without overburden (OB) using the CORSIKA-CMC-FLUKA sample. Rates shown correspond to 211 seconds in real time (or equivalently to 1.32E12 beam spills).

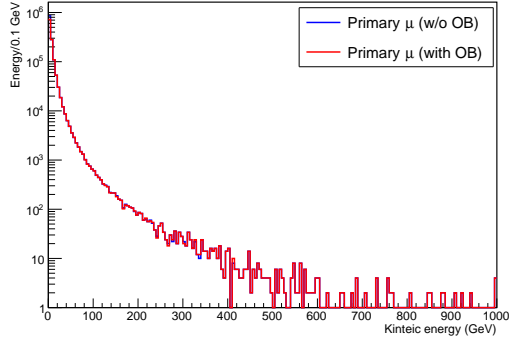
Table 12 shows the effect of overburden on primary (CRY air showers) and secondary backgrounds that enter the active volume of the detector. Rates shown in the table correspond to 211 seconds in real time. One has to look at columns 2 and 3 in the table to see the effect of the included overburden. The biggest effect of overburden is on primary neutrons, protons and electromagnetic background, reducing them by about 76%, 98% and 81% respectively. As expected, primary muons are mildly affected by the concrete overburden (only reduced by about 9%).

Table 12 also shows the indirect effect of an overburden on secondary particle rates. In particular, secondary neutron and proton production is reduced significantly ($\sim 62\%$ to $\sim 72\%$) due to the reduction in the primary neutron background. Please note here that the secondary neutron/proton rates shown in the table are *not* corrected for the fact that Geant4 often gives new track IDs to particles that scatter (see Appendix A for more details). Most of the secondary electromagnetic background seen in the table is induced by primary muons. With the inclusion of the overburden, these rates are reduced by about $\sim 9\%$ to $\sim 16\%$ which roughly matches with the reduction in the primary muon rate due to overburden. As discussed elaborately in Section 6.1, this is an inevitable background MicroBooNE will see irrespective of whether an overburden will be installed or not. The importance of estimating the ν_e -like background and methods to reduce them is discussed in the same section. Figure 19 shows the energy distribution of various backgrounds (both primary and secondary) that enter the active volume of the detector with and without overburden using the nominal sample.

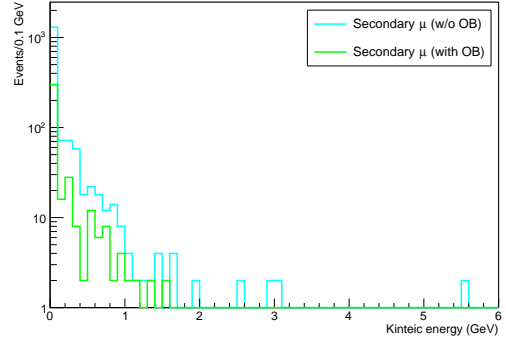
From the discussion above, one can infer that a 3 m overburden is very effective in reducing the non-muon primary background (especially primary neutrons and protons). But, before making a decision, it is important to verify that the overburden does not cause damage to MicroBooNE's physics program, particularly the EM-excess measurement. Most importantly, the following two questions need to be addressed:

- How does an overburden effect the cosmogenic ν_e -like background? In other words, we want to verify that the secondary production in the overburden doesn't significantly increase this background.
- Undoubtedly, the overburden must be producing secondaries in its volume, but what ultimately matters is the size of these secondary backgrounds (most importantly if the produced background is ν_e -like) that enter the active volume of the detector.

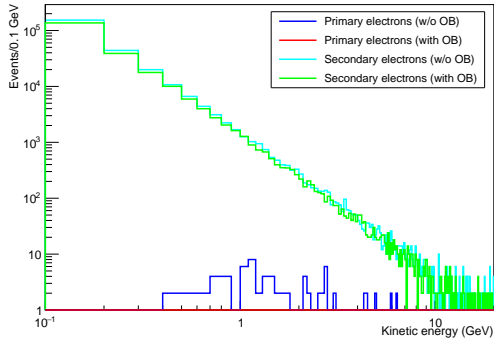
Both questions are dealt in detail in Sections 7.1 and 7.2, respectively.



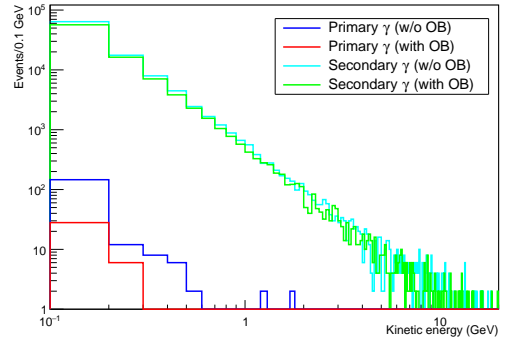
(a) Primary Muons



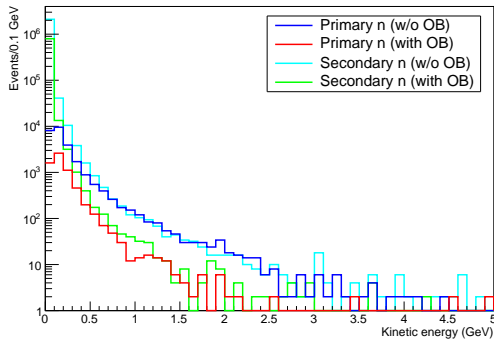
(b) Secondary Muons



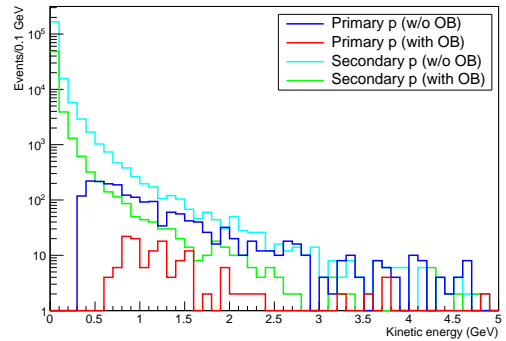
(c) Electrons



(d) Photons



(e) Neutrons



(f) Protons

Figure 19: Energy distribution of various cosmic particles that enter the TPC with and without overburden simulation using the CORSIKA-CMC-FLUKA sample. Particles coming from primary (CRY output) and secondary (Geant4) processes are separated to show the effect of overburden separately. In the plots, *OB* is used as a short form for overburden. Also, in the case of muons, photons and electrons, a 100 MeV cut is implemented. Please note the difference in axes scales between the plots.

467 7.1 Effect of overburden on cosmogenic ν_e -like backgrounds

468 Cosmogenic ν_e -like backgrounds are described in Section 6.1. In order to see the effect of an overburden
 469 on these backgrounds, the analysis shown in Section 6.1 is repeated with the overburden cosmic sam-
 470 ple. Table 13 shows how the ν_e -like background rates vary with the inclusion of overburden (compare
 471 columns 2 and 3 in the table). Column 4 in the table shows the significance of difference between
 472 both cases in terms of σ . As expected, the overburden causes large reductions in non-muon-induced
 473 backgrounds and modest reductions to muon-induced backgrounds.

474

Process	Particle rate (w/o overburden)	Particle rate (with overburden)	Significance of difference (in σ)
Compton in spill, primary μ in AV	318 \pm 23	265 \pm 21	-1.69
Pair production in spill, primary μ in AV	15917 \pm 162	15539 \pm 161	-1.67
Compton in spill, primary μ not in AV	3	0	–
Pair production in spill, primary μ not in AV	71 \pm 11	28 \pm 7	-3.30
Primary γ Compton in spill	3.3	0	–
Primary γ pair production in spill	231 \pm 20	6.6	-11.2
Compton in spill, primary is not a μ or γ	28 \pm 7	1.7	-3.76
Pair production in spill, primary is not a μ or γ	1474 \pm 49	244 \pm 20	-23.2

Table 13: Cosmogenic ν_e -like background rates ($E > 200$ MeV), with and without overburden simulation, occurring in the detector fiducial volume as defined in Section 6.1. AV here stands for active volume of the detector. For convenience, rates are shown for 1.32E12 beam spills which correspond to 3 years of BNB run.

475 This is a positive result showing that the chosen overburden configuration doesn't increase the ν_e -like
 476 background rate. It actually reduces the non-muon-induced backgrounds significantly. The next section
 477 shows what portion of this ν_e -like background is directly induced by the overburden.

478 7.2 Secondary production in the overburden

479 The concrete overburden is located ~ 14 meters from the top surface of the MicroBooNE detector. A
 480 large amount of absorptive material surrounds the detector in this gap, such as the walls, platform,
 481 electronics racks, cryogenic piping and the passive portions of the cryostat. Any secondary production
 482 due to interactions in the overburden would need to survive all this material before it can reach the
 483 detector. Also, the overburden itself has a thickness of 3 m which makes it possible to re-absorb most
 484 of the background that it creates.

485

486 In order to understand how these features affect particle propagation, the end point distribution of
 487 all particles that are created in the overburden is plotted. Figure 20 shows this distribution in the YX
 488 (left) and YZ (right) projection of the detector. Most of the background created in the overburden gets
 489 re-absorbed in the overburden and for most of what is left, the surrounding material does a good job
 490 of absorbing it. One can see from the figure that only a little of this background reaches the detector.
 491 Figure 21 shows the same set of plots (as in Figure 20) but with an energy cut of 100 MeV which further
 492 suppresses this background.

493

494 The ν_e -like background that originates from interactions in the overburden is also calculated and
 495 found to be negligible. Out of the total background shown in Table 13, *only* 10 ± 4 events are directly
 496 induced by the overburden which shows that an overburden of 3 m doesn't increase the overall ν_e -like

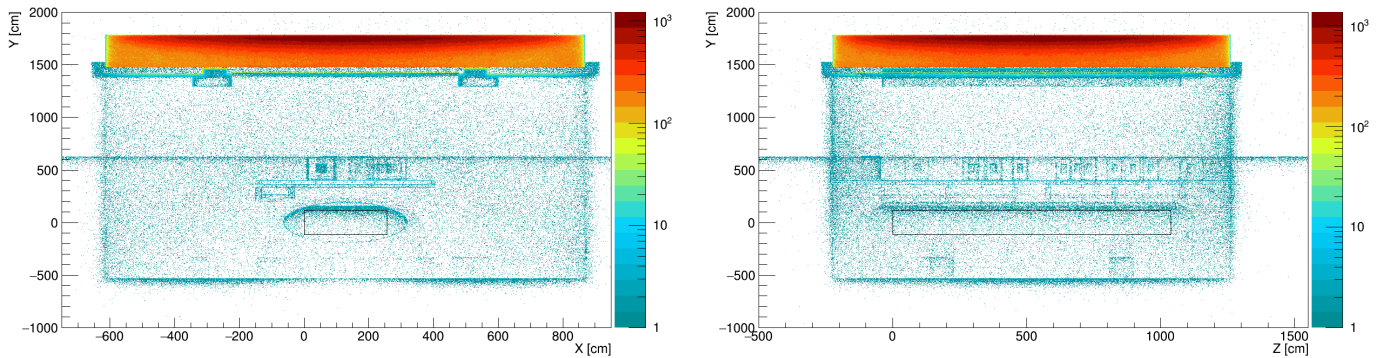


Figure 20: End point distribution of all cosmic particles that are created in the 3 m concrete overburden. Left (right) plot shows the distribution in the YX (YZ) projection of the MicroBooNE TPC. Plots correspond to 10,000 cosmic events (64 seconds real time).

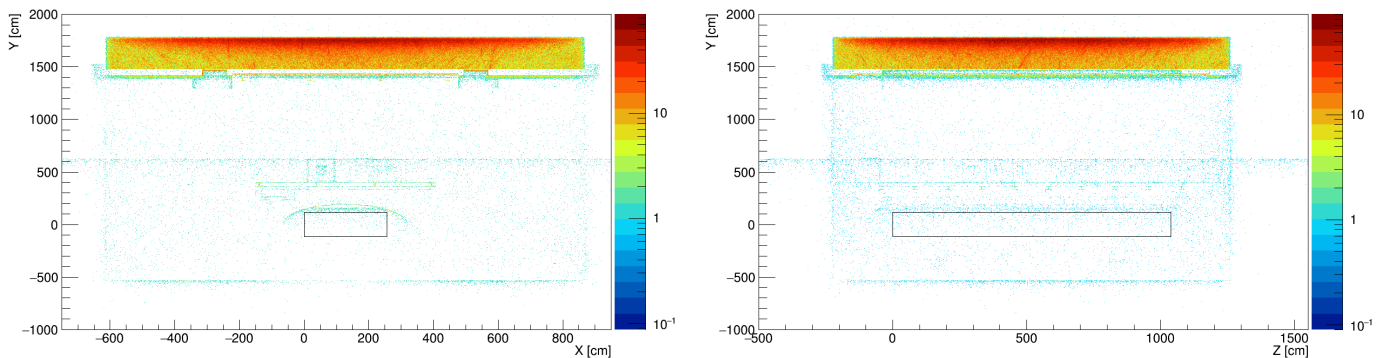


Figure 21: End point distribution of all cosmic particles that are created in the 3 m concrete overburden. A 100 MeV energy cut is applied on all particles. Left (right) plot shows the distribution in the YX (YZ) projection of the MicroBooNE TPC. Plots are made using 10,000 events which correspond to 64 seconds in real time.

497 background. Figure 22 (left) shows the end point distribution of all EM particles contained in ν_e -like
 498 showers that originate in the overburden. Figure 22 (right) shows the start point distribution of ν_e -like
 499 showers that are daughters of photons created in the overburden.

500 7.3 Overburden size recommendation

501 Although the overburden studies shown in this document are done using a 3 m thick concrete disc, for
 502 technical and cost reasons, it is important to determine whether a thinner slab would do a similar job
 503 of shielding cosmic particles. This question is addressed in this section. To understand the absorption
 504 per unit length in the overburden for various particles, one can look at the distance of a particle end
 505 point on the Y-axis from the top of the overburden. Figure 23 shows the distribution of distance of pri-
 506 mary and secondary particle end points from the top surface of the overburden for various particle types.
 507

508 From the left column of Figure 23, one can see that in the case of primary particles, an overburden
 509 of 1 m (for protons and γ) to 1.5 m (for neutrons) thickness absorbs most of the background. But, the
 510 overburden should also be thick enough to reabsorb most of the secondary production that happens in
 511 the overburden itself. The right column of Figure 23 shows that the effect of an overburden plateaus
 512 around 2 m. In summary, two meter and three meter overburdens have similar shielding efficiency.

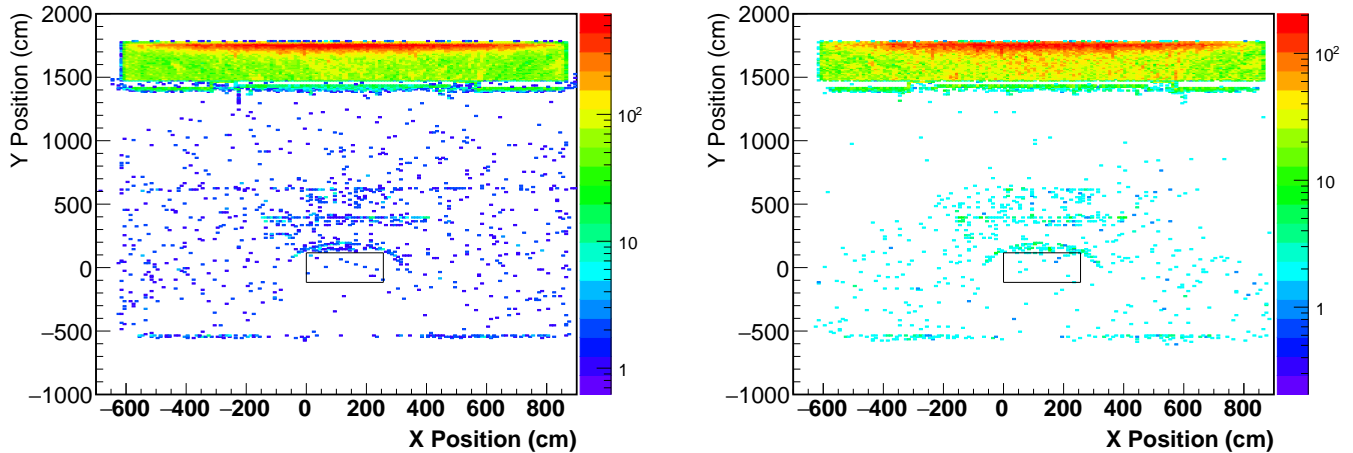


Figure 22: End point distribution of all EM particles contained in ν_e -like showers that are created in the 3 m concrete overburden (Left). Startpoint distribution of ν_e -like showers that are daughters of photons created in the 3 m concrete overburden (Right). plots show the distributions in the YX projection of the MicroBooNE TPC.

8 Summary and conclusions

Using MC Truth information, the size of various cosmic backgrounds expected in the MicroBooNE detector are calculated. The effect of a 3 m concrete overburden on various particle rates is studied in detail. Based on the studies presented in this note, the following observations are made:

- The CORSIKA simulation with the 5-component CMC and FLUKA hadron-interaction models gives best estimate of the cosmic background expected in the MicroBooNE detector.
- The primary motivation for an overburden is to shield non-muon primaries and any backgrounds triggered by them. A 3 m concrete overburden reduces the non-muon background by about 76% to 92% (see Table 12). Muons and muon-induced secondaries are mildly reduced by the overburden (by up to about 9%) and carefully-devised cuts are required to identify and reject muon-induced ν_e -like backgrounds.
- The ν_e -like background induced by non-muon primaries is several times larger than the expected intrinsic ν_e charged-current signal and the low energy excess signal (see Table 9). A 3 m concrete overburden significantly (84% to 97%) reduces the Compton and pair-produced backgrounds induced by non-muon primaries and marginally (2% for pair production showers, 17% for Compton showers) reduces the background induced by a crossing muon.
- Most of the background that gets recreated in the overburden is absorbed in the overburden. Only a negligible portion of this background enters the detector.
- Most importantly, the overburden decreases the observed ν_e -like background.

Another important thing to note here is that all background numbers shown in this document are to be considered as a lower bound as they are expected to get worse due to the following reasons:

- In the case of neutrons, Geant4 has the tendency to count scattered primaries as secondaries, so, the primary neutron numbers shown in this document are actually underestimated⁷ which makes

⁷Initial estimates show that the neutron rate is underestimated by four times due to this.

536 the need for an overburden even more important.

537 • When presenting background numbers for beam-integrated times, 100% out of the spill rejection
 538 efficiency is assumed which is not true in reality.

539 • The ν_e intrinsic charged-current signal numbers and low energy excess numbers shown in Table 9
 540 are calculated assuming 80% flat reconstruction efficiency. But in reality the shower reconstruction
 541 efficiencies do not perform well for energies below 200 MeV.

542 • One can argue that the cosmic mitigation studies show good rejection efficiency for ν_e -like showers,
 543 but these studies are performed with truth information and assuming a 94% flat efficiency in
 544 identifying pair-produced showers. There is no strong basis for the 94% efficiency assumption.

545 All of the above reasons make the impact of overburden even more important for MicroBooNE. Looking
 546 at Table 13, the size of non-muon induced ν_e -like background that reaches the detector after the 3 m

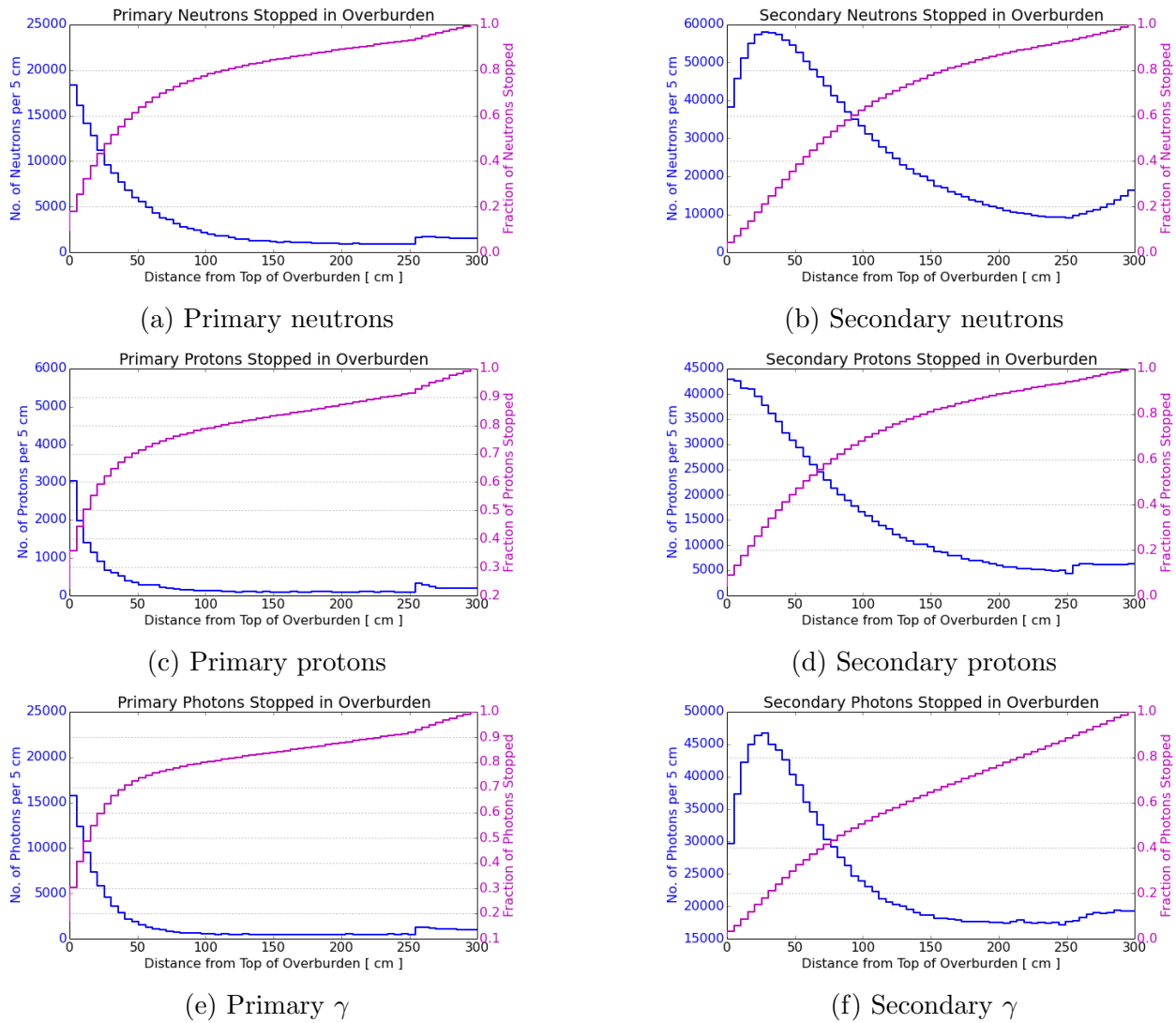


Figure 23: Distance of end Y positions of various particles from the top surface of the overburden. The set of plots on the left correspond to primary particles and the set of plots on the right correspond to secondary particles. Plots are made using the nominal CORSIKA-CMC-FLUKA sample with 10,000 events.

547 concrete shielding is comparable to the size of the signal events. But, the point of overburden is that
548 it reduces the ν_e -like background to a manageable level which can then be further reduced using the
549 mitigation cuts described in Ref. 21.

550
551 Given the arguments presented in this section, *the cosmogenics task force strongly recommends that*
552 *MicroBooNE install a concrete overburden of at least two meters to reliably control cosmic non-muon*
553 *induced ν_e -like backgrounds and successfully perform MicroBooNE's flagship physics analysis.*

554 9 Acknowledgments

555 We thank everyone who helped us directly or indirectly during the course of this study. We would like
556 to specifically thank R. Guenette, C. James, B. J. P. Jones, V. Kudryavtsev, A. Szelc, M. Weber and
557 J. Zennamo, for productive discussions and putting forward interesting questions which greatly helped
558 these studies. We would also like to thank B. Fleming, G. Zeller and M. Weber for their excellent
559 leadership and organization on the MicroBooNE experiment.

560 References

- 561 [1] *Cosmic-ray shower generator (CRY) for Monte Carlo transport codes*, Nuclear Science Symposium
562 Conference Record, 2007. NSS '07. IEEE (Volume: 2).
563 *CRY* : [http : //nuclear.llnl.gov/simulation/main.html](http://nuclear.llnl.gov/simulation/main.html)
- 564 [2] *CORSIKA an Air Shower Simulation Program*
565 [https : //web.ikp.kit.edu/corsika/usersguide/usersguide.pdf](https://web.ikp.kit.edu/corsika/usersguide/usersguide.pdf)
- 566 [3] GEANT4 Collaboration, S. Agostinelli *et al.*, *GEANT4: A Simulation toolkit*
567 Nucl. Instrum. Meth. A **506** (2003) 250-303.
- 568 [4] S. Gollapinni *et al.*, AnalysisTree documentation wiki page
569 [https : //cdcv.s.fnal.gov/redmine/projects/uboonecode/wiki/AnalysisTree_variables](https://cdcv.s.fnal.gov/redmine/projects/uboonecode/wiki/AnalysisTree_variables)
- 570 [5] S. Gollapinni *et al.*, MicroBooNE DocDB 3943.
- 571 [6] Eric D. Church, *LArSoft: A Software Package for Liquid Argon Time Projection Drift Chambers*,
572 arXiv:1311.6774 [physics.ins-det].
- 573 [7] Robert K Kutschke, *art: A Framework for New, Small Experiments at Fermilab*,
574 J. Phys.: Conf. Ser. **331** (2011) 032019.
- 575 [8] J. F. Ziegler, *Terrestrial cosmic ray intensities*, IMB J. Res. Develop. 42 (1) (January 1998), 117-139.
- 576 [9] MCNPX User's Manual, Version 2.5.0, Laurie Waters, *ed.*, LA-CP-05-0369 (2005).
577 [http : //mcnpx.lanl.gov/documents.html](http://mcnpx.lanl.gov/documents.html)
- 578 [10] R. Grosso, *Cosmic stopped muon rates*, MicroBooNE DocDB# 2673.
- 579 [11] K. Woodruff, *Studies of the Cosmic ray flux in MicroBooNE*, MicroBooNE DocDB# 3351.
- 580 [12] L. Kalousis, *Cosmic muon flux measurements at the Liquid Argon Test Facility (LArTF)*,
581 MicroBooNE Technote DocDB# 3130.

- 582 [13] B. Eberly, *Muon flux validation*, MicroBooNE DocDB# 3842.
- 583 [14] D. Caratelli, *Cosmogenics update*, MicroBooNE DocDB# 3882.
- 584 [15] S. Gollapinni, *Buffer box studies*, MicroBooNE DocDB# 3831.
- 585 [16] S. Tognini, S. C. Gomes, *CORSIKA Converter Tool*, R. A. HEP Group, Federal University of
586 Goias, Brazil. stognini@fnal.gov and ragomes@if.ufg.br. November 2014.
- 587 [17] C. Forti, H. Bilokon, B. d’Ettore Piazzoli, T. K. Gaisser, L. Satta and T. Stanev, *Simulation of*
588 *atmospheric cascades and deep underground muons*, Phys. Rev. D **42**, 3668 (1990).
- 589 [18] Bhadra, Arunava and Ghosh, Sanjay K. and Joarder, Partha S. and Mukherjee, Arindam and
590 Raha, Sibaji, *Study of low energy hadronic interaction models based on BESS observed cosmic ray*
591 *proton and antiproton spectra at medium high altitude*, Phys. Rev. D **79**, 114027 (2009).
- 592 [19] R. Acciarri (3) *et al.*, *arXiv:1503.01520*
- 593 [20] D. Kaleko, *Low Energy Excess: MiniBooNE to MicroBooNE*, MicroBooNE DocDB# 3862.
- 594 [21] D. Caratelli *et al.*, *Electron-neutrino appearance cosmogenic background mitigation in MicroBooNE*,
595 MicroBooNE Technote# 3978-v2.

597 **Neutron and Proton scattering in Geant4**

598 As noted in Section 6, it is a known fact that Geant4 often assigns new track IDs to particles that
 599 scatter. When computing secondary particle rates, especially for particles like neutrons and protons
 600 where one can end up overestimating the rates. It is not totally clear under what conditions Geant4
 601 assigns a new track ID to the track segments belonging to the same particle. One can guess that the
 602 magnitude of scattering angle or the energy lost between the intermediate processes could trigger this
 603 behavior from Geant4. In AnalysisTree, there is a provision to identify such cases using a variable
 604 called *MergedId*. All Geant track segments, which belong to the same particle, are assigned the same
 605 *MergedId*. Using this variable and using a CRY sample, we tried to estimate how often this happens in
 606 the case of neutrons and protons.

607
 608 Figure 24 (left) shows the number of Geant track segments belonging to the same neutron that get
 609 assigned a new track ID from Geant4. Figure 24 (right) shows the same distribution for protons. From
 610 these figures, it is clear that neutrons are greatly affected by this feature in Geant4 and most neutrons
 611 have at least one scattered track segment that Geant assigns a new track ID to. Table 14 shows the
 612 secondary rates for neutrons and protons before and after the Geant4 correction. One can see from
 613 the table that if not corrected for this behavior in Geant4, one will end up overcounting the secondary
 614 neutron rate by about 40 to 45% and proton rate by about 5 to 7%.

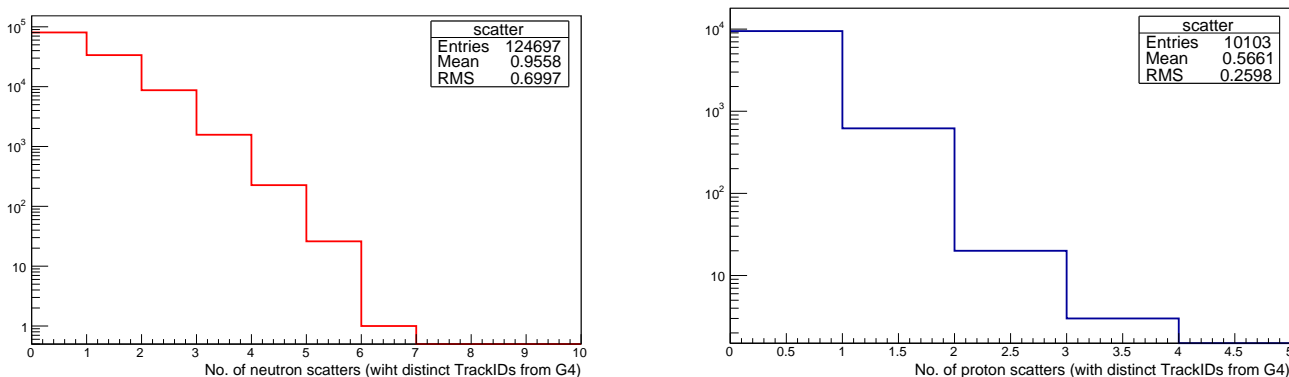


Figure 24: Distribution of number of Geant track segments belonging to the same neutron (left) and same proton (right) that get a new track ID from Geant4 (only computed for particles that enter the TPC active volume). Plots are shown for a CRY sample with no overburden simulation. Plots are made using 40,000 events which correspond to 256 seconds in real time.

Particle type	Particle rate (w/o OB)	
	(before)	(after)
neutron	102778	55931
proton	8327	7777

Table 14: Secondary particle rates expected in the TPC active volume for neutrons and protons before and after the Geant4 correction. Rates are shown using a CRY sample with no overburden simulation. Rates shown correspond to 211 seconds in real time (or equivalently to 1.32E12 beam spills).

615 Appendix B

616 Neutron “Killer” processes in LArG4

617 The neutron killer process can be turned off by removing the *NeutronTrackingCut* option in the LArG4
 618 physics list. The MicroBooNE specific physics list is defined in *uboone/Utilities/services_microboone_simulation.f*
 619 file:

```
620 microboone_g4_services.LArG4Parameters.UseCustomPhysics: true
621 microboone_g4_services.LArG4Parameters.EnabledPhysics: [ "Em",
622                                                         "FastOptical",
623                                                         "SynchrotronAndGN",
624                                                         "Ion",
625                                                         "Hadron",
626                                                         "Decay",
627                                                         "HadronElastic",
628                                                         "Stopping",
629                                                         "NeutronTrackingCut" ]
```

630 The *NeutronTrackingCut* is what enables the neutron killer process which kills neutrons after 10 μ s.
 631 Table 15 shows how this process affects the neutron rate for MicroBooNE for various CORSIKA con-
 632 figurations. As an example, in Figure 25, we show the energy distribution of primary and secondary
 633 neutrons and protons with and without the neutron killer process using a CRY sample.

Particle type	CORSIKA(Proton) FLUKA (before nkiller)	CORSIKA(Proton) FLUKA (after nkiller)	CORSIKA(CMC) GHEISHA (before nkiller)	CORSIKA(CMC) GHEISHA (after nkiller)	CORSIKA(CMC) FLUKA (before nkiller)	CORSIKA(CMC) FLUKA (after nkiller)
neutron	4.62	10.75	2.52	5.99	5.89	13.77
proton	0.46	0.97	0.24	0.54	0.60	1.25

Table 15: Number of primary plus secondary particles expected in the TPC active volume per 1.6 ms time window for neutrons and protons with and without the neutron killer process. Numbers are shown for various CORSIKA generator configurations. In this case, the geometry simulation doesn’t include any type of overburden.

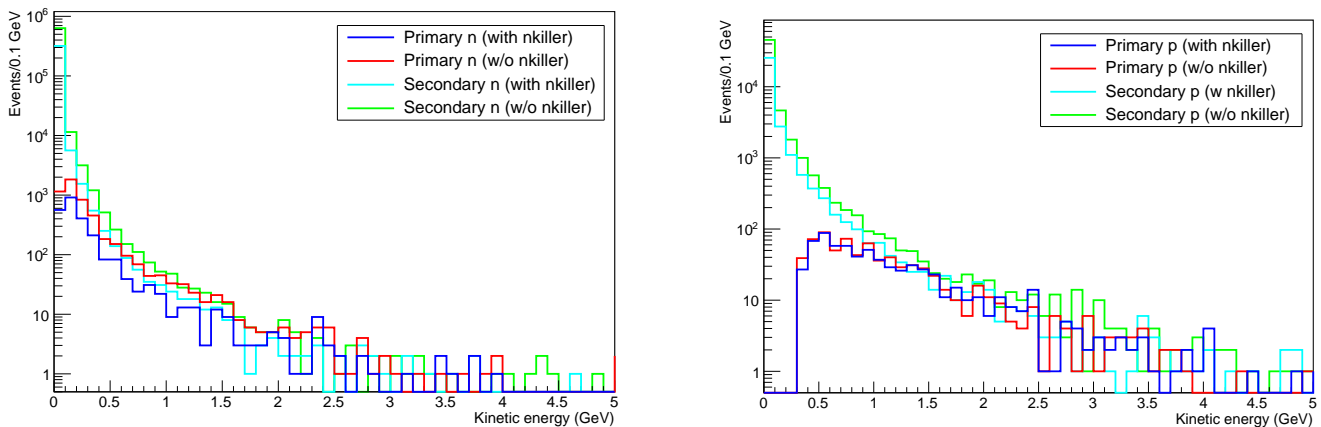


Figure 25: Energy distribution of CRY primary and secondary neutrons (left) and protons (right) with and without the neutron killer process.